I

Publication I

K. J. Jalkanen, V. W. Jurgensen and I. M. Degtyarenko, *Linear response properties required to simulate vibrational spectra of biomolecules in various media: (R)-Phenyloxirane (a comparative theoretical and spectroscopic vibrational study)*, Advances in Quantum Chemistry **50**, 91-124 (2005).

Linear Response Properties Required to Simulate Vibrational Spectra of Biomolecules in Various Media: (R)-Phenyloxirane (A Comparative Theoretical and Spectroscopic Vibrational Study)

K.J. Jalkanen[1], V. Würtz Jürgensen[1] and I.M. Degtyarenko[2]

[1]*Quantum Protein (QuP) Center, Department of Physics, Technical University of Denmark, Building 309, DK-2800 Lyngby, Denmark*
E-mails: jalkanen@fysik.dtu.dk, wuertz@fysik.dtu.dk
[2]*Laboratory of Physics, Helsinki University of Technology, P.O. Box 1100, FIN-02015 Espoo, Finland*
E-mail: imd@fyslab.hut.fi

Abstract

We here present a combined VA, VCD, Raman and ROA vibrational study of phenyloxirane. We have simulated the vibrational absorption (VA), also called IR, vibrational circular dichroism (VCD), Raman scattering and Raman optical activity (ROA) intensities utilizing the density functional theory (DFT) B3LYP hybrid exchange correlation functional and other exchange-correlation functionals (PBE, PW91, PBE1) with the 6-31G(d,p), 6-31++G(d,p), cc-pVDZ, aug-cc-pVDZ, cc-pVTZ and augmented correlation consistent polarized valence triple zeta (aug-cc-pVTZ) basis sets. Previously authors have focused on either the VA and VCD spectra or the Raman and ROA spectra of molecules, since the experimental and theoretical instruments and methods for calculating these quantities are quite distinct. Here we show that the combined analysis gives more information, especially with respect to the electric dipole, magnetic dipole, electric dipole – electric dipole polarizability, electric dipole – electric quadrupole polarizability and electric dipole – magnetic dipole polarizability changes during the various induced transitions. The coupling of vibrational and electronic excitations may be used to aid in understanding the photo induced chemical reactivity observed in many systems. This work is a continuation of our goal to interpret the results of experimental studies on the basis of theoretical results, which can help to understand the structure and function of proteins, other biomolecules and ligands in their native environments. As the physical tools used to observe and study biological processes have evolved, so have the theoretical methods and models to interpret, understand and completely utilize the results of these new measurements. The work on developing methods for modeling amino acids, peptides, proteins and ligands in both the non aqueous (lipid) and aqueous environments has involved, of course, many groups. A review of our contributions to this field has recently been presented. In addition to interpreting existing and new experimental results, we will discuss structural, energetic, conformational, and vibrational studies on a variety of systems that have been used to test and validate levels of theory, and in addition to suggest modifications to existing levels of theory, which can make them even more useful than they currently are.

Contents

ADVANCES IN QUANTUM CHEMISTRY, VOLUME 50
ISSN: 0065-3276 DOI: 10.1016/S0065-3276(05)50006-6

1. INTRODUCTION

Ashvar and coworkers have recently presented the vibrational absorption (VA) and vibrational circular dichroism (VCD) spectra for a variety of rigid ring systems and compared their density functional theory (DFT) calculations with their experimental measurements [10,12,11,9]. The currently implemented methods to calculate the atomic polar and atomic axial tensors seem to be able to reproduce the VA and VCD intensities quite well. Previously both Stephens and coworkers and Suhai and coworkers have shown that an accurate geometry and Hessian are the most critical parameters. Without a good experimental or theoretical geometry and an accurate representation of the normal modes as derived from the Hessian, one is not able to accurately predict either the absolute VA and VCD intensities or even the relative intensities [72,76,83,132,27,52,51,73]. Hence the question of finding and developing methods that can accurately predict and find the experimental structure are very important also in the field of modeling and studying small to medium sized pharmaceutical molecules, as they are in protein and ligand modeling. In the protein modeling field people have used the known NMR and X-ray structures in the Worldwide Protein Data Bank (wwPDB) to try to predict and(or) find the structures of closely related sequences of proteins [26]. Here the two main methods are the so called homology method and the neural network method [99]. Extensive reviews of both methods have occurred and hence there is no need to elaborate or go into detail.

The use of other experimental data has also been used to try to shine some light on the structure determination problem. For example, electronic circular dichroism (ECD), VA, and Raman spectroscopy have been used to try to determine the amount of secondary structural elements in a given new protein, where the X-ray or NMR structures are not yet available [104,136,138,98]. In addition to these three methods, two relatively new methods have recently been able to make contributions, VCD and ROA [85,84,22]. Even through these two methods were both experimentally developed and the first spectra measured in the 1970s [69,68,18,20], only recently has the interpretation of the VA and VCD intensities in strongly perturbing environments been shown to be feasible [60,137,52,74,75]. Previously the theory of VCD has been put on a firm basis [35,130,131,28] similar to that for VA [114,161]. In addition, to the rigorous theoretical basis for the VA and VCD intensities, the implementation at the restricted Hartree–Fock (RHF), multi configuration self consistent field (MCSCF) and DFT levels utilizing finite difference techniques, coupled Hartree–Fock and the random phase approximation have been reported [2,134,4,5,79,62, 15,16,14,30,29]. The theory of Raman scattering has been also put on a rigorous theoretical basis [57,97]. The EDEDP and their derivatives with respect to nuclear displacements that are necessary to simulate the Raman scattering spectra have been implemented at the RHF and DFT levels [89,3,81].

In addition, a rigorous theory of Raman optical activity has been derived by Barron and Buckingham [19] and been implemented by finite difference techniques utilizing Amos's implementation of the electric dipole – magnetic dipole polarizabilities (EDMDP) and

electric dipole – electric quadrupole polarizabilities (EDEQP) in the Cambridge Analytical Derivatives Package (CADPAC) [1] by Polavarapu and Jalkanen [116,21,159,38,60, 74], subsequently implemented in the Dalton program by Helgaker, Bak, Ruud, Jørgensen and Olsen [67,119] and in latest release of Gaussian [54]. Here we look at the combination of VA, VCD, Raman scattering and ROA spectroscopies to explore the properties of phenyloxirane.

2. METHODS AND MATERIALS

In this work we have optimized the geometry of phenyloxirane at the B3LYP/6-31++G(d,p) level of theory with Gaussian 03 [54]. At this same level of theory we have additionally calculated the Hessian, the atomic polar tensors (APT), the atomic axial tensors (AAT), and the electric dipole – electric dipole polarizability derivatives (EDEDPD), which allows us to simulate the VA, VCD and Raman spectra. In addition we have calculated the EDMDP and EDEQP at the optimized geometry and at the displaced geometries that has allowed us to calculate the EDMDP and EDEQP derivatives, EDMDPD and EDEQPD, respectively. We have used the two point finite difference to calculate the derivatives with respect to the nuclear Cartesian coordinates. By having these quantities and the EDEDPD, we can additionally simulate the ROA spectra. The EDMDP and EDEQP were all calculated at the RHF/6-31G(d,p) level with the Cambridge Analytical Derivatives Package (CADPAC), version 5.2 provided to us by Nick Handy and Roger Amos [6,1]. In addition, we have calculated the EDEDPD, EDMDPD and the EDEQPD at the B3LYP level of theory with the 6-31G(d,p) and aug-cc-pVDZ basis sets, which allows us to also simulate the ROA spectra at this level of theory. We have utilized the finite difference methods and the gauge invariant atomic orbitals (GIAO) method to calculate the EDMDP at the displaced geometries as implemented in Gaussian 03 RevC.02 [54]. This is similar to the implementation for the calculation of the ROA spectra available in the Dalton program [67,119].

In addition, we have calculated the VA, VCD, and Raman spectra at the PBE, PW91 and PBE1 levels of theory with the correlation consistent polarized valence triple zeta (aug-cc-pVTZ) basis set. Furthermore we have investigated the basis set dependence of the VA, VCD and Raman spectra at the B3LYP level of theory; the basis sets being compared are the 6-31G(d,p), 6-31++G(d,p), cc-pVDZ, aug-cc-pVDZ, cc-pVTZ and aug-cc-pVTZ [86, 43,53,33,66]. Note that the cc-pVTZ and aug-cc-pVTZ are relatively large basis sets and are used to benchmark the lower basis set level calculations, as these large basis sets are not feasible for doing complete potential energy surfaces scans including the VA, VCD, Raman and ROA spectra at all points. Hence it is important to compare the quality for both the 6-31G(d,p) [split valence plus polarization functions] and 6-31++G(d,p) [split valence plus diffuse functions plus polarization functions] basis sets, the level of agreement with both the larger basis sets and the experimental spectra being the measures. The cc-pVXZ, X = D and T, are the correlation consistent polarized valence double (D)and triple (T) zeta basis sets developed in the group of Dunning [43]. In addition, they have extended these basis sets to treat anions, electron affinities and weakly bonded systems (H-bonding and dispersion energies) by adding additional diffuse functions to generate the aug-cc-pVXZ, X = D and T [86]. For the helium dimer, it has been shown that aug-cc-pVTZ basis sets or larger are necessary to get qualitative results that can be used to extrapolate to the CBS limit for the binding energy (well depth), equilibrium bond length and the harmonic frequency.

The helium dimer is a very rigorous test for both the *ab initio* or DFT levels of theory. It has been shown that Møller Plesset perturbation theory to fourth order (MP4) or coupled cluster that includes all single and double excitations and a posteriori perturbative correction for connected triple excitations [CCSD(T)] level *ab initio* levels of theory are necessary. The MP2, MP3 and CCSD levels of theory are inadequate in order to get quantitative results for these properties [142]. Hence the need to find and document DFT exchange correlation functionals that are of equivalent accuracy to the MP4 and CCSD(T) or better are required, since MP4 and CCSD(T) *ab initio* levels of theory are computationally very demanding. The results, however, at these levels of theory can be used to benchmark many properties. In addition, they have been used to benchmark linear response properties as well, *e.g.*, the calculation of polarizabilities and hyperpolarizabilities, and reaction barrier heights where it was shown that aug-cc-pVXZ basis sets must be used to get quantitative accuracy [115,151].

Therefore, in addition, we have also determined the optimized structure of phenyloxirane with the B1B95 exchange correlation functional and the TPSS meta-GGA exchange correlation functional as implemented in Gaussian 03 with the aug-cc-pVTZ basis set [129, 24]. This basis set or a higher level correlation consistent basis set should be used to check the accuracy of the new DFT GGA, meta GGA, hybrid and meta hybrid functionals [160, 36,148,115].

Finally utilizing the SIESTA (Spanish Initiative for Electronic Simulations with Thousands of Atoms) program we have at the PBE level of theory with the DZP basis set optimized the structure of phenyloxirane. Details of SIESTA relaxation (geometry optimizations) are as follows. In order to determine the equilibrium structure, we relax all the atomic coordinates (that is, reduce the size of the forces (gradients) on each atom) with a conjugate gradient algorithm, reaching a tolerance in the forces of 0.04 eV Å^{-1}. We use the fully self-consistent density functional method implemented in the SIESTA program [105, 127]. The electronic energy is obtained within general gradient approximation (GGA) as parametrized by Perdew, Burke and Ernzerhof [109,110]. Core electrons were replaced by nonlocal Troullier–Martins [139] norm-conserving pseudopotentials, whereas valence electrons are described in terms of linear combination of numerical pseudoatomic orbitals of the Sankey type [123,124]. In these calculations we used the double-ζ plus polarization basis set, it provides a sufficiently accurate description of the system that we intend to study. Real space integrations were performed on a regular grid with an equivalent cutoff of 150 Ry.

We assume here that the basis set dependence for the various exchange correlation GGA functionals and hybrid methods, mega hybrid methods, double hybrid methods and double meta hybrid methods will be approximately the same [160], but these remain to be thoroughly investigated. Clearly the state of the art of DFT simulations for molecular properties, which include the effects due to the solvent and protein environment where hydrogen bonding and dispersion forces are important, is in a state of high activity and fluctuation. We do not here investigate all of the recent developments with respect to both the development of exchange-correlation functionals and the developments of methods to treat response properties, but rather take the pragmatic approach of showing that current methods do now exist in three programs, which allow one to calculate the VA, VCD, Raman and ROA spectra to a high degree of accuracy, being CADPAC, Gaussian 03 or Dalton.

As new DFT GGA and hybrid exchange correlation functionals are developed, of course the best ones need to be implemented and tested for all of the pieces needed to simulate these spectra, that is, the geometries, relative energies, gradients, Hessians, the electric dipole moments, the magnetic dipole moments, the EDEDP, the EDMDP and the EDEQP and their derivatives with respect to nuclear displacement. In addition, how all of these quantities change with changes in the environment needs to be taken into account, both implicitly and explicitly and probably both. Finally the effects due to temperature and the frequency of the radiation also need to be taken into account, possibly with time dependent DFT and its various implementations, be it Car Parinello molecular dynamics (CPMD) or Born Oppenheimer quantum molecular dynamics (BOQMD). In this work, however, we do not take these parameters into account. Since the Raman and ROA spectra are not resonance enhanced, that is, the radiation used for the Raman and ROA measurements was not close to an electronic transition, this approximation is OK. But clearly, if one wishes to simulate the resonance Raman and resonance ROA spectra, the frequency of the incoming radiation must be treated theoretically via time dependent DFT. Here the exchange correlation functionals must satisfy the additional constraint that they also treat excited states correctly. This is an even more serious problem for many of the currently used exchange correlation functionals and their modifications and their combinations with exact exchange. A detailed discussion of this problem is also beyond the scope of this work.

3. RESULTS

3.1. Structure

In Table 1 we present the geometrical parameters for the B3LYP optimized structures of phenyloxirane with the 6-31G(d,p), 6-31++G(d,p), cc-pVDZ, aug-cc-pVDZ, cc-pVTZ and aug-cc-pVTZ basis sets [95,23]. In addition, we present the geometrical parameters presented by Ashvar and coworkers [10]. The atom numbering in Table 1 is shown in Fig. 1. In addition, we present the optimized structure of phenyloxirane calculated at the PBE level of theory with the Dunning double zeta polarized basis set. Finally, we also present the optimized structures of phenyloxirane at the PBE, PBE1, PW91, B1B95 and TPSS levels of theory with the aug-cc-pVTZ basis set [109,110,112,108,24,129]. Here we investigate the effect of changing the exchange correlation functional on the geometrical properties.

As one can see by comparing our calculated geometrical parameters at the B3LYP level of theory with the various basis sets with those presented recently by Ashvar and coworkers [10], the structures are very similar. The effect of the diffuse functions seems to be to make the bond lengths in the benzene ring a bit longer (6-31++G(d,p)). In addition, we have investigated the effects of changing the DFT exchange correlation functional at the aug-cc-pVTZ basis set level, the largest differences being between the results for PBE1 and B1B95 exchange correlation functional and with those for the B3LYP hybrid exchange correlation functional. For example, the C1–O3 (C2–O3) bonds in the oxirane ring are shorter by 0.012 (0.13) and 0.013 (0.09) Å, while the C1–C2 bond is only shorter by 0.006 and 0.006 Å, for the PBE and B1B95 methods with respect to the B3LYP method with the aug-cc-pVTZ basis set, respectively. The C2–C10 bond from the oxirane ring to the benzene ring is

Table 1. Structural parameters for (R)-phenyloxirane for various basis sets for B3LYP level of theory and additionally for the PBE, PBE1, PW91, B1B95 and TPSS levels of theory with the aug-cc-pVTZ basis set

	B3LYP [10] TZ2P [10]	PBE DZP	B3LYP G(d,p)	B3LYP ppG(d,p)	B3LYP ccpVDZ	B3LYP AccpVDZ	B3LYP ccpVTZ	B3LYP AccpVTZ	PBE AccpVTZ	PBE1 AccpVTZ	PW91 AccpVTZ	B1B95 AccpVTZ	TPSS AccpVTZ
$r_{1,3}$	1.430	1.453	1.430	1.429	1.431	1.436	1.427	1.427	1.434	1.415	1.434	1.414	1.437
$r_{2,3}$	1.433	1.460	1.435	1.433	1.433	1.441	1.431	1.433	1.444	1.420	1.444	1.422	1.448
$r_{1,2}$	1.474	1.498	1.478	1.476	1.480	1.479	1.472	1.472	1.479	1.466	1.478	1.466	1.477
$r_{2,10}$	1.488	1.506	1.492	1.490	1.494	1.493	1.488	1.486	1.488	1.482	1.486	1.480	1.489
$r_{9,10}$	1.395	1.422	1.400	1.398	1.402	1.402	1.395	1.395	1.401	1.391	1.400	1.388	1.400
$r_{8,9}$	1.390	1.416	1.395	1.393	1.397	1.398	1.389	1.390	1.396	1.387	1.395	1.385	1.395
$r_{7,8}$	1.390	1.417	1.396	1.394	1.398	1.398	1.390	1.390	1.396	1.387	1.395	1.385	1.395
$r_{7,12}$	1.391	1.418	1.397	1.394	1.399	1.400	1.391	1.391	1.398	1.388	1.397	1.387	1.397
$r_{11,12}$	1.389	1.416	1.394	1.392	1.397	1.397	1.389	1.389	1.395	1.386	1.393	1.383	1.393
$r_{10,11}$	1.395	1.421	1.400	1.398	1.402	1.403	1.395	1.395	1.402	1.391	1.401	1.389	1.401
$\theta_{1,3,2}$	62.0	61.9	62.1	62.1	62.2	61.9	62.0	61.9	61.8	62.3	61.8	61.8	61.6
$\theta_{3,1,2}$	59.1	59.3	59.1	58.8	59.0	59.2	59.1	59.2	59.4	59.0	59.4	59.6	59.6
$\theta_{3,2,1}$	58.9	58.8	58.8	59.1	58.8	58.9	58.9	58.8	58.8	58.7	58.8	58.6	58.9
$\theta_{3,2,10}$	117.8	117.8	117.6	117.6	117.5	117.7	117.9	117.9	117.8	117.7	117.6	117.2	117.4
$\theta_{1,2,10}$	122.5	121.9	122.2	122.2	122.0	122.6	122.5	122.7	122.4	122.1	122.4	121.6	122.5
$\theta_{2,10,9}$	119.5	119.5	119.8	119.7	120.0	119.5	119.6	119.5	119.6	119.7	119.6	120.2	119.7
$\theta_{2,10,11}$	121.3	121.2	120.9	121.1	120.8	121.4	121.3	121.4	121.3	121.1	121.3	120.5	121.2
$\theta_{8,9,10}$	120.6	120.5	120.5	120.5	120.5	120.6	120.6	120.6	120.6	120.5	120.6	120.4	120.5
$\theta_{7,8,9}$	120.1	120.1	120.1	120.1	120.1	120.1	120.1	120.1	120.1	120.1	120.1	120.1	120.1
$\theta_{8,7,12}$	119.6	119.7	119.7	119.7	119.7	119.6	119.6	119.6	119.7	119.7	119.7	119.7	119.7
$\theta_{7,12,11}$	120.3	120.3	120.3	120.3	120.3	120.4	120.3	120.3	120.3	120.3	120.3	120.2	120.3
$\theta_{10,11,12}$	120.3	120.2	120.3	120.3	120.3	120.3	120.3	120.3	120.3	120.3	120.3	120.3	120.3
$\theta_{9,10,11}$	119.1	119.3	119.2	119.2	119.2	119.1	119.1	119.1	119.1	119.2	119.1	119.3	119.1
$\tau_{3,1,2,10}$	105.2	−105.3	−104.9	−105.1	−104.9	−104.9	−105.3	−105.1	−105.1	−105.1	−105.1	−104.5	−104.7
$\tau_{3,2,10,9}$	163.9	164.3	165.2	168.0	169.0	160.9	161.7	161.7	159.1	162.5	159.0	157.2	158.0
$\tau_{3,2,10,11}$	16.4	−16.3	−15.4	−12.6	−11.2	−19.4	−18.7	−18.7	−21.3	−18.0	−21.4	−23.4	−22.4
$\tau_{1,2,10,9}$	126.9	−126.9	−126.1	−123.1	−122.4	−130.1	−129.1	−129.1	−132.0	−128.9	−132.1	−134.6	−133.1

(*continued on next page*)

Table 1. (*Continued*)

	B3LYP [10] TZ2P [10]	PBE DZP	B3LYP G(d,p)	B3LYP ppG(d,p)	B3LYP ccpVDZ	B3LYP AccpVDZ	B3LYP ccpVTZ	B3LYP AccpVTZ	PBE AccpVTZ	PBE1 AccpVTZ	PW91 AccpVTZ	B1B95 AccpVTZ	TPSS AccpVTZ
$\tau_{1,2,10,11}$	52.7	52.5	59.3	56.3	57.5	49.7	50.5	50.5	47.7	50.7	47.6	44.8	46.5
$\tau_{8,9,10,2}$	178.7	178.8	178.6	178.5	178.9	178.8	178.8	178.8	178.7	178.7	178.7	178.6	178.7
$\tau_{2,10,11,12}$	178.9	−179.1	−178.7	−178.8	−179.0	−179.1	−179.1	−179.0	−179.0	−178.9	−179.0	−178.8	−179.0
$\tau_{7,8,9,10}$	0.6	0.5	0.5	0.5	0.5	0.6	0.5	0.5	0.5	0.5	0.5	0.4	0.5
$\tau_{12,7,8,9}$	0.2	−0.1	0.2	0.1	0.2	0.1	0.1	0.1	0.2	0.2	0.2	0.1	0.2
$\tau_{8,7,12,11}$	0.4	−0.2	−0.4	−0.4	−0.4	−0.4	−0.4	−0.4	−0.4	−0.4	−0.4	−0.3	−0.4
$\tau_{10,11,12,7}$	0.0	0.1	−0.1	0.0	−0.1	0.0	0.0	0.0	0.0	0.0	0.0	−0.0	−0.0
$\tau_{9,10,11,12}$	0.7	0.3	0.7	0.6	0.8	0.7	0.7	0.6	0.7	0.7	0.7	0.6	0.7
$\tau_{8,9,10,11}$	0.9	−0.6	−0.9	−0.9	−1.1	−1.0	−0.9	−0.9	−0.9	−0.9	−0.9	−0.8	−0.9
$\tau_{6,2,10,9}$	25.6	25.0	26.4	29.4	29.9	22.9	23.5	23.5	20.6	23.6	20.6	18.4	20.2

The B3LYP/TZ2P results are taken from Ref. [10]. The PBE/DZP results are from the SIESTA program. All other results are from the Gaussian 03.

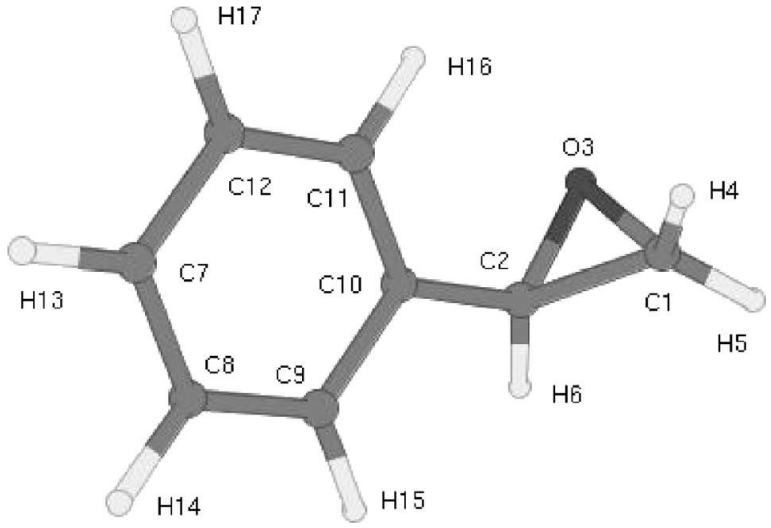

Fig. 1. (R)-Phenyloxirane structure, atom numbering for Table 1.

shorter by 0.004 and 0.006 Å for the PBE and B1B95 levels of theory with respect to the B3LYP level of theory. In the benzene ring, the C–C bond lengths are approximately all 0.003–0.004 Å shorter for PBE1, but a bit shorter for B1B96, being 0.003–0.006 Å, with respect to the B3LYP level of theory.

In contrast, the C1–O3 (C2–O3) bond lengths in the oxirane ring are calculated to be longer with the PBE, PW91, and TPSS levels (of theory), now being 0.007 (0.011), 0.007 (0.011) and 0.010 (0.015) Å for the PBE, the PW91, and the TPSS levels with respect to the B3LYP level, respectively. The C1–C2 bond length in the oxirane ring is also longer, 0.007, 0.006 and 0.005 Å with respect to the PBE, the PW91, and the TPSS levels, respectively. The C2–C10 bond from the oxirane ring to the benzene ring is 0.002, 0.000 and 0.003 Å longer for the PBE, the PW91, and the TPSS levels with respect to the B3LYP level, respectively. In the benzene ring, the CC bond lengths are longer by 0.006–0.007 Å for PBE, 0.005–0.006 Å for PW91 and 0.005–0.006 Å for TPSS. Note that the PBE, PW91 and TPSS levels give very similar results, as do the PBE1 and B1B95 levels, with the B3LYP level giving results in between these two extremes. With respect to the benzene ring CC bond lengths, the PBE, PW91 and TPSS levels give very similar bond lengths, with the PBE1 and B1B95 giving shorter values, and B3LYP giving intermediate lengths. The valence angles are all very similar at all the levels. The largest differences are seen in the SIESTA PBE results. Here the bond lengths in the oxirane ring are more than 0.1 Å longer than those calculated with the PBE level with the larger basis set, aug-cc-pVTZ. Note that in the SIESTA calculations, we use pseudopotentials, whereas in the Gaussian calculations we do not.

With respect to the basis set effect at the B3LYP level, the largest effect is seen with augmenting (addition of diffuse functions) the cc-pVDZ basis, with the two C–O ring bond lengths increasing by 0.005 and 0.007 Å, respectively. By contrast, the ring CC bond decreases by only 0.001 Å. We have optimized the geometry of the (R)-phenyloxirane, while Ashvar and coworkers have the (S)-enantiomer, as seen by, *e.g.*, $\tau_{3,1,2,10}$, being −105.1 for us (B3LYP/6-31++G(d,p)), and 105.2 by them. This will of course give us the opposite sign for all of the VCD and ROA intensities. Similarly the other dihedral angles, $\tau_{3,2,10,11}$ and $\tau_{3,2,10,9}$ are of opposite sign, again reflecting the opposite enantiomer. $\tau_{3,2,10,11}$ has

values ranging from −11.2 for the cc-pVDZ basis set to −19.4 with the aug-cc-pVDZ basis, reflecting the large effect of adding the diffuse functions to the cc-pVDZ basis set at the B3LYP level. Note the value of this angle has not changed with the addition of the diffuse functions to the cc-pVTZ basis set, the value being −18.7 in both cases. At the other DFT levels of theory (exchange correlation functionals) the value of this torsion angle varies from −18.0 at the PBE1 level to −23.4 with the B1B95 level, while the PBE, PW91 and TPSS levels give −21.3, −21.4 and −22.4, respectively, again all with the aug-cc-pVTZ basis set.

In the next four subsection, we discuss our simulated VA, VCD, Raman scattering, and ROA spectra and compare them to recent calculations and measurements of the VA and VCD spectra of Ashvar and coworkers [10] and Raman and ROA measurements by Hecht and Barron [64,63]. In addition, we shall try to see how the changes in geometry that we see with the different DFT exchange correlation functional are reflected in these spectra, and ultimately which structural parameters are reflected in the various vibrational spectra.

3.2. Vibrational absorption

In Fig. 2 we present our simulated B3LYP VA spectra for phenyloxirane with various basis sets. Our simulated spectra are very similar to the simulated VA spectra of Ashvar and coworkers, which were also calculated at the B3LYP level of theory but with a different basis set, the so called TZ/2P basis set developed by Amos and Handy and a part

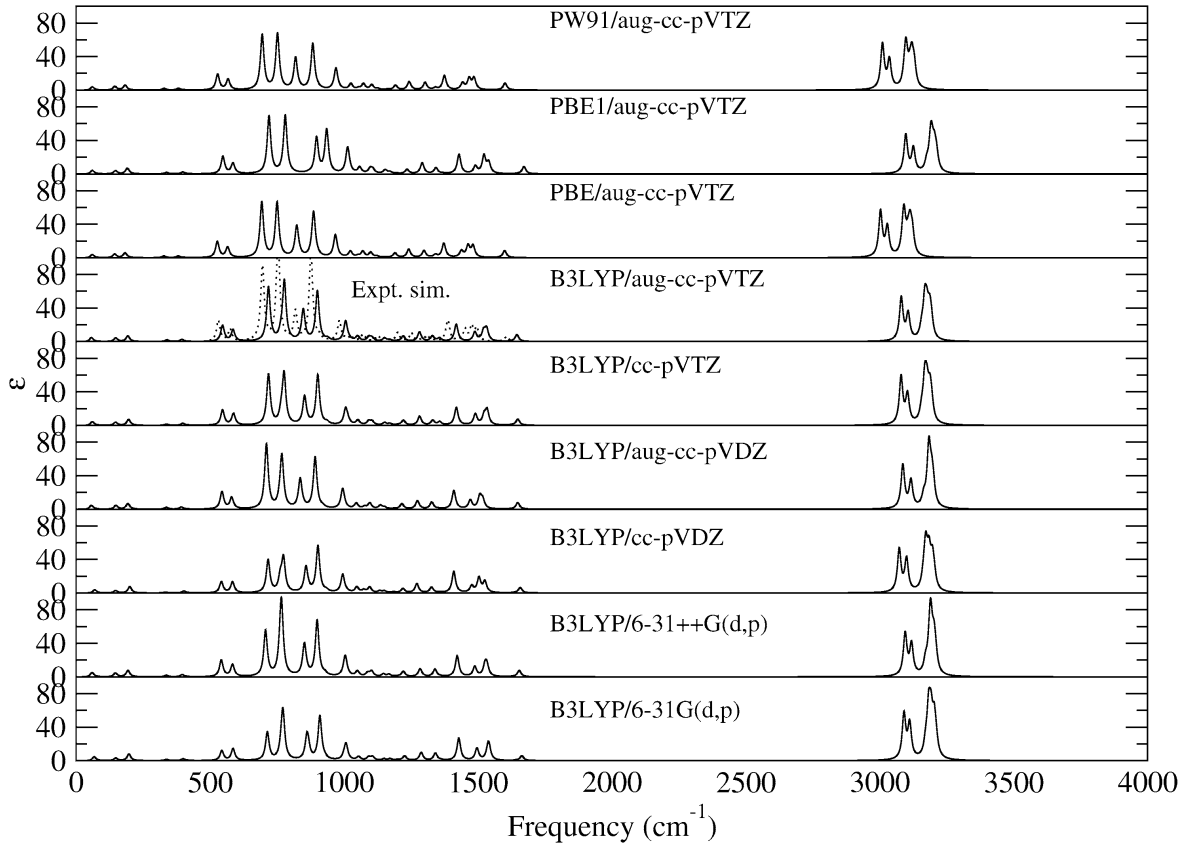

Fig. 2. Phenyloxirane VA spectra for various DFT methods.

of the CADPAC basis set library [133,6]. In addition, we present the simulated VA spectra calculated at the PBE, PBE1 and PW91 levels (of theory) with the largest basis set, aug-cc-pVTZ. We also use the reported experimental frequencies and dipole strengths to simulate the experimental spectra of Ashvar. Here we use a line width of 8 cm^{-1} for our Expt. sim. also reported in Fig. 2. All of the spectra calculated at the B3LYP level are very similar, as we have performed calculations only with polarized spit valence quality of basis set (6-31G(d,p), that is, the so called polarization d functions on carbon and oxygen and polarization p functions on hydrogen) or better. Of course, increasing the quality of the basis set has led to an improvement in the quality of the calculation and representation of the experimental spectra, but the main features of the spectra are well represented already with the 6-31G(d,p) basis set at the B3LYP level. This is consistent with previous works performed in Stephens' group where they showed that the main effect is adding the polarization functions to the split valence basis sets, the effects of further increases are much smaller. Previously Pulay and workers have recommended the use of only split valence basis sets for geometry optimizations and frequency calculations, but the split valence basis sets are not of sufficient accuracy for the VA intensities, that is, for the calculation of the APT [114].

Hence the geometry and Hessian calculated with the 6-31G(d,p) basis set and an appropriate *ab initio* or DFT level of theory are accurate and can be used to also predict the VCD, Raman and ROA intensities, given that the required tensors are calculated (which normally require a larger basis set, that is, the APT, AAT, EDEDPD, EDMDPD and EDEQPD). The VA intensities are more sensitive to the changes in the coupling in the off diagonal elements of the vibrational coordinate force constants than the vibrational frequencies [76]. This is due to mixing of the internal coordinates. The VA intensities have been shown to be very sensitive to the accuracy of the force field, especially the off diagonal force constants [132,76,72]. The VA intensities require the calculation of the APT in addition to the Hessian [114]. This is a real test of the accuracy of the force field, much better than just the root mean square (RMS) deviation of the calculated harmonic and experimental frequencies. Note also that the experimental frequencies are anharmonic and the calculated frequencies are harmonic.

The bands that were most affected by changing the basis set from 6-31++G(d,p) to aug-cc-pVTZ were those calculated at 1361 and 1357 cm^{-1} where the intensity changes from 0.7 to 6.7 (experimental 1329 cm^{-1} with intensity being 3.6), the pair at 1006/1002 cm^{-1} and 1018/1006 cm^{-1} where the intensities are 47.4/10.9 and 1.9/54.2 (only one band being found in the experiment at 983 cm^{-1} with intensity 56.5), 763 and 765 cm^{-1} but with intensities 54.8 and 18.7 (experimental 752 cm^{-1} with intensity 96.3). Hence in some cases the smaller basis set gave better agreement than the larger basis set. With respect to the change in the exchange correlation functional at the highest basis set level, the PBE and PW91 frequencies and intensities are very similar, while the B3LYP and PBE1 are very similar. The relative order of the CH stretch modes are different comparing the two sets, reflecting small changes in the force constants, both diagonal and off-diagonal elements. In the mid IR the PBE and PW91 mode calculated at 1600 and 1602 cm^{-1}, respectively, are closer to the experimental value at 1608 cm^{-1}, than the B3LYP and PBE1 values of 1646 and 1672 cm^{-1}, respectively. But since the experimental values are anharmonic and all of our calculated values are harmonic, this better agreement for this one mode may not reflect an overall better accuracy. The vibrational frequencies can be correlated with

the geometries, and the similarities in the spectra with respect to the different functionals appear to also reflect the aforementioned differences in the geometries.

In Table 2 we present the calculated vibrational frequencies and dipole strengths (used to simulate the VA intensities) at the B3LYP level using the 6-31++G(d,p) and aug-cc-pVTZ basis sets. In addition we present the simulated VA spectra calculated also at the B3LYP level, but with the 6-31G(d,p), cc-pVDZ, aug-cc-pVDZ and cc-pVTZ basis sets in Fig. 2. These simulations show that the simulations of the VA spectra with these basis sets (that is, cc-pVDZ, aug-cc-pVDZ and cc-pVTZ) are not greatly different than the two presented in Table 2 (that is, 6-31++G(d,p) and aug-cc-pVTZ). The fine features of the spectra change, the major features are very similar. In addition, we also present the calculated vibrational frequencies and dipole strengths at the PBE, PBE1 and PW91 levels at the highest basis set level we used in this study, that is, the aug-cc-pVTZ, in Table 2. The spectral simulations for these other DFT levels of theory are also given in Fig. 2. Here we can see that the changes in the spectra with respect to changing the exchange correlation functional (levels of theory) are larger than the changes with respect to basis set for the B3LYP level of theory.

3.3. Vibrational circular dichroism

In Fig. 3 we present our simulated VCD spectra for (R)-phenyloxirane with various basis sets at the B3LYP DFT level along with the corresponding experimentally simulated spectra for (S)-phenyloxirane (Expt. sim.). Here we use the frequencies and rotational strengths extracted from the experimental spectra by Ashvar and coworkers for our experimental simulated spectra and spectra line width of 8 cm^{-1}. Note that the experimental spectra is not complete, as the experimental setup does not allow a complete VCD spectra to be measured. There is good agreement between our simulated VA and VCD spectra and that of Ashvar and coworkers [10] as shown in Figs. 3 and 8 (discussed later). The agreement between the calculated and measured VCD intensities is a further confirmation of a good geometry and Hessian as can be seen comparing our simulated spectra in Figs. 3 and 8 with the experimental spectra presented in Figs. 4, 5, 7 and 8 of Ref. [10] and our experimental simulated spectra presented also in Figs. 3 and 8. In addition, we present our predicted VCD spectra calculated with the aug-cc-vPTZ basis set at the PBE, PBE1 and PW91 levels of theory. The main features of the VCD spectra are all well produced with the high quality aug-cc-pVTZ basis set and these four DFT levels of theory. The VCD intensities, like the VA intensities are very sensitive to the force field and it has been shown that the most sensitive part of the VA and VCD intensity calculations is having an accurate geometry and Hessian [132,72]. The nature of the normal modes are tested by their ability to accurately simulate the VA and VCD intensities, given accurate APT and AAT [130,134,4,77,131,28, 78,5,79,62,15,16,14,30].

In Table 3 we present the calculated vibrational frequencies and rotational strengths (used to simulate the VCD intensities) with the B3LYP hybrid DFT method using the 6-31++G(d,p) and aug-cc-pVTZ basis sets. In addition we present the simulated VCD spectra calculated also with the B3LYP hybrid DFT method but with the 6-31G(d,p), cc-pVDZ, aug-cc-pVDZ and cc-pVTZ basis sets in Fig. 3. These simulations also show that the simulations of the VCD spectra with these basis sets (*i.e.*, cc-pVDZ, aug-cc-pVDZ and cc-pVTZ) are not very different than the two simulations for which the rotational strengths

Table 2. Comparison of vibrational frequencies and VA intensities for phenyloxirane

	$\bar{\nu}$ (cm^{-1}) B3LYP ppGdp	($\bar{\nu}$ (cm^{-1})) exp [10]	D_i B3LYP ppGdp	(D_i) exp [10]	$\bar{\nu}$ (cm^{-1}) B3LYP AccpVTZ	D_i	$\bar{\nu}$ (cm^{-1}) PBE AccpVTZ	D_i	$\bar{\nu}$ (cm^{-1}) PBE1 AccpVTZ	D_i	$\bar{\nu}$ (cm^{-1}) PW91 AccpVTZ	D_i
r_1	3209.		12.0		3193.	12.8	3122.	17.3	3212.	13.2	3129.	17.3
r_2	3203.		23.9		3186.	20.0	3113.	24.4	3204.	17.1	3120.	24.3
r_3	3192.		26.6		3176.	19.5	3105.	11.4	3195.	12.6	3112.	10.8
r_4	3188.		32.8		3169.	30.7	3096.	0.2	3191.	26.6	3103.	0.2
r_5	3181.		0.6		3166.	0.2	3091.	35.0	3185.	0.2	3098.	34.1
r_6	3171.		9.8		3157.	8.3	3086.	7.5	3176.	7.2	3093.	7.8
r_7	3119.		26.8		3106.	22.9	3029.	26.2	3126.	21.3	3036.	25.7
r_8	3095.		37.1		3081.	38.1	3003.	41.4	3098.	33.7	3011.	40.8
r_9	1655.	(1608.)	10.4	(7.5)	1646.	11.2	1600.	11.9	1672.	11.8	1602.	11.8
		(1601.)		(1.3)								
r_{10}	1633.	(1586.)	0.3	(0.1)	1625.	0.4	1581.	0.2	1651.	0.3	1582.	0.2
r_{11}	1534.	(1496.)	17.3	(3.1)	1533.	21.2	1482.	20.8	1541.	18.7	1486.	21.1
r_{12}	1527.	(1477.)	19.1	(26.9)	1521.	16.9	1464.	21.3	1523.	31.5	1468.	20.1
r_{13}	1489.	(1452.)	17.9	(22.2)	1489.	16.3	1439.	12.0	1491.	13.3	1443.	12.5
r_{14}	1423.	(1389.)	40.1	(35.9)	1419.	33.1	1373.	28.5	1430.	37.1	1375.	28.6
		(1383.)		(9.7)								
r_{15}	1361.	(1329.)	0.7	(3.6)	1357.	6.7	1342.	5.4	1370.	0.8	1342.	4.0
		(1311.)		(9.7)								
r_{16}	1340.	(1295.)	14.6	(4.9)	1330.	10.7	1299.	14.2	1344.	12.0	1303.	15.4
		(1288.)		(0.8)								
r_{17}	1285.	(1252.)	16.6	(18.3)	1282.	19.9	1242.	18.1	1292.	23.2	1245.	18.0
r_{18}	1222.	(1201.)	11.4	(19.6)	1221.	11.7	1191.	10.2	1236.	9.3	1194.	10.7
r_{19}	1201.	(1177.)	0.9	(2.0)	1200.	0.9	1160.	1.2	1196.	1.3	1163.	1.2
r_{20}	1184.	(1157.)	0.3	(1.8)	1182.	0.3	1144.	0.3	1177.	0.2	1148.	0.3
r_{21}	1168.	(1144.)	5.0	(8.1)	1171.	3.3	1123.	2.9	1171.	3.8	1126.	2.8
r_{22}	1147.	(1126.)	5.7	(11.1)	1152.	7.7	1100.	12.2	1154.	8.8	1104.	12.0
		(1106.)		(0.6)								
r_{23}	1103.	(1077.)	12.9	(6.3)	1104.	8.2	1071.	15.2	1108.	9.6	1073.	15.1

(*continued on next page*)

Table 2. (*Continued*)

	$\bar{\nu}$ (cm^{-1}) B3LYP ppGdp	($\bar{\nu}$ (cm^{-1})) exp [10]	D_i B3LYP ppGdp	(D_i) exp [10]	$\bar{\nu}$ (cm^{-1}) B3LYP AccpVTZ	D_i	$\bar{\nu}$ (cm^{-1}) PBE AccpVTZ	D_i	$\bar{\nu}$ (cm^{-1}) PBE1 AccpVTZ	D_i	$\bar{\nu}$ (cm^{-1}) PW91 AccpVTZ	D_i
r_{24}	1089.	(1069.)	8.5	(12.1)	1093.	10.3	1051.	3.4	1098.	12.0	1054.	3.4
r_{25}	1050.	(1026.)	13.4	(12.5)	1051.	12.6	1024.	15.9	1059.	15.3	1026.	15.8
r_{26}	1014.	(1002.)	1.2	(2.6)	1021.	1.5	990.	0.2	1023.	0.2	993.	0.2
r_{27}	1006.	(983.)	47.4	(56.5)	1018.	1.9	974.	3.4	1020.	5.5	977.	2.7
r_{28}	1002.		10.9		1006.	54.2	968.	61.1	1014.	67.4	970.	59.0
r_{29}	986.	(966.)	0.1	(0.2)	999.	0.1	955.	0.3	1002.	0.0	958.	0.3
r_{30}	929.	(909.)	5.9	(9.9)	939.	6.2	900.	3.1	941.	11.1	902.	3.2
r_{31}	900.	(877.)	169.7	(275.5)	901.	152.3	887.	140.4	935.	119.2	885.	141.9
r_{32}	862.		5.4		867.	0.8	833.	5.9	898.	108.0	834.	1.6
r_{33}	852.	(819.)	100.8	(96.1)	848.	100.2	824.	101.5	869.	1.3	820.	105.5
r_{34}	767.	(755.)	237.6	(270.5)	778.	209.5	751.	199.0	781.	202.3	752.	202.8
r_{35}	763.	(752.)	54.8	(96.3)	765.	18.7	744.	1.4	772.	2.4	746.	0.9
r_{36}	708.	(696.)	176.3	(295.3)	718.	205.8	693.	218.8	720.	219.0	695.	217.1
		(673.)		(2.3)								
		(664.)		(0.4)								
		(655.)		(0.7)								
r_{37}	631.	(619.)	0.1	(0.1)	634.	0.1	610.	0.2	629.	0.2	613.	0.2
r_{38}	584.	(575.)	55.7	(57.3)	586.	52.9	566.	49.3	586.	47.9	567.	50.0
r_{39}	542.	(531.)	83.4	(109.3)	547.	79.9	527.	82.7	548.	86.3	529.	81.4
r_{49}	416.		1.6		418.	1.4	400.	1.9	416.	1.3	401.	1.9
r_{41}	396.		14.9		395.	14.7	381.	12.0	398.	12.8	382.	12.4
r_{42}	337.		12.7		339.	13.3	328.	14.3	338.	12.3	329.	14.7
r_{43}	194.		90.3		193.	78.3	183.	72.1	191.	81.7	183.	72.4
r_{44}	147.		69.5		148.	66.5	144.	69.0	147.	59.4	145.	70.7
r_{45}	59.		200.8		57.	191.5	60.	146.2	60.	162.9	60.	148.0

Table 3. Comparison of vibrational frequencies and VCD intensities for (R)-phenyloxirane, experimental data was for (S)-phenyloxirane

	$\bar{\nu}$ (cm^{-1}) B3LYP ppGdp	($\bar{\nu}$ (cm^{-1})) exp [10]	R_i B3LYP ppGdp	(R_i) exp [10]	$\bar{\nu}$ (cm^{-1}) B3LYP AccpVTZ	R_i	$\bar{\nu}$ (cm^{-1}) PBE AccpVTZ	R_i	$\bar{\nu}$ (cm^{-1}) PBE1 AccpVTZ	R_i	$\bar{\nu}$ (cm^{-1}) PW91 AccpVTZ	R_i
r_1	3209.		−1.7		3193.	−2.2	3122.	−1.9	3212.	−1.7	3129.	−1.9
r_2	3203.		0.4		3186.	0.6	3113.	0.6	3204.	0.8	3120.	0.5
r_3	3192.		−0.1		3176.	1.1	3105.	1.6	3195.	0.8	3112.	1.6
r_4	3188.		4.5		3169.	3.6	3096.	0.5	3191.	3.1	3103.	0.5
r_5	3181.		0.2		3166.	−0.1	3091.	3.0	3185.	0.3	3098.	3.0
r_6	3171.		0.4		3157.	0.7	3086.	1.0	3176.	0.6	3093.	1.0
r_7	3119.		4.4		3106.	3.3	3029.	3.1	3126.	3.3	3036.	2.9
r_8	3095.		0.9		3081.	1.5	3003.	1.3	3098.	−0.2	3011.	1.7
r_9	1655.	(1608.) (1601.)	0.7		1646.	0.6	1600.	0.7	1672.	0.6	1602.	0.7
r_{10}	1633.	(1586.)	−0.1		1625.	−0.3	1581.	−0.1	1651.	−0.2	1582.	−0.1
r_{11}	1534.	(1496.)	1.4	(−1.6)	1533.	0.6	1482.	0.4	1541.	1.8	1486.	0.4
r_{12}	1527.	(1477.)	13.3	(−7.5)	1521.	12.4	1464.	15.4	1523.	15.7	1468.	14.7
r_{13}	1489.	(1452.)	2.2	(−9.7)	1489.	3.2	1439.	0.9	1491.	1.9	1443.	1.2
r_{14}	1423.	(1389.) (1383.)	6.2	(−8.6) (3.8)	1419.	5.0	1373.	7.1	1430.	1.1	1375.	6.9
r_{15}	1361.	(1329.) (1311.)	−0.1	(−4.2) (−2.2)	1357.	4.4	1342.	−8.8	1370.	−5.1	1342.	−7.7
r_{16}	1340.	(1295.) (1288.)	−4.0	(8.3) (0.8)	1330.	−9.4	1299.	2.1	1344.	2.2	1303.	1.6
r_{17}	1285.	(1252.)	−17.8	(26.0)	1282.	−19.3	1242.	−25.4	1292.	−25.6	1245.	−25.2
r_{18}	1222.	(1201.)	7.9	(−16.2)	1221.	9.2	1191.	9.4	1236.	9.9	1194.	9.4
r_{19}	1201.	(1177.)	−0.8	(0.4)	1200.	−0.6	1160.	−0.8	1196.	−0.7	1163.	−0.8
r_{20}	1184.	(1157.)	−0.1	(−0.1)	1182.	−0.1	1144.	−0.1	1177.	−0.1	1148.	−0.1
r_{21}	1168.	(1144.)	0.6	(2.6)	1171.	−0.1	1123.	0.9	1171.	−1.9	1126.	0.9
r_{22}	1147.	(1126.) (1106.)	5.2	(−19.4)	1152.	8.5	1100.	13.6	1154.	10.8	1104.	13.4
r_{23}	1103.	(1077.)	1.5	(−2.8)	1104.	1.4	1071.	0.6	1108.	1.5	1073.	0.7

(*continued on next page*)

Table 3. (*Continued*)

	$\bar{\nu}$ (cm^{-1}) B3LYP ppGdp	($\bar{\nu}$ (cm^{-1})) exp [10]	R$_i$ B3LYP ppGdp	(R$_i$) exp [10]	$\bar{\nu}$ (cm^{-1}) B3LYP AccpVTZ	R$_i$	$\bar{\nu}$ (cm^{-1}) PBE AccpVTZ	R$_i$	$\bar{\nu}$ (cm^{-1}) PBE1 AccpVTZ	R$_i$	$\bar{\nu}$ (cm^{-1}) PW91 AccpVTZ	R$_i$
r_{24}	1089.	(1069.)	−0.3	(−0.4)	1093.	−0.5	1051.	−1.0	1098.	0.3	1054.	−1.0
r_{25}	1050.	(1026.)	0.6	(−1.2)	1051.	0.3	1024.	0.2	1059.	0.2	1026.	0.2
r_{26}	1014.	(1002.)	−0.5	(0.7)	1021.	−0.7	990.	−0.1	1023.	0.1	993.	−0.1
r_{27}	1006.	(983.)	47.4	(14.4)	1018.	0.04	974.	−0.3	1020.	−0.4	977.	−0.2
r_{28}	1002.		−2.7		1006.	−11.0	968.	−15.5	1014.	−14.0	970.	−14.9
r_{29}	986.	(966.)	0.0		999.	0.1	955.	0.04	1002.	0.1	958.	0.0
r_{30}	929.	(909.)	1.1		939.	0.8	900.	2.0	941.	−0.4	902.	1.7
r_{31}	900.	(877.)	−8.0		901.	−6.9	887.	−7.0	935.	−4.3	885.	−7.1
r_{32}	862.		−8.2		867.	−3.8	833.	−8.3	898.	2.8	834.	−4.8
r_{33}	852.	(819.)	16.0		848.	15.2	824.	17.9	869.	3.0	820.	15.6
r_{34}	767.	(755.)	−12.0		778.	−22.7	751.	−27.3	781.	−21.6	752.	−28.4
r_{35}	763.	(752.)	−21.5		765.	−12.1	744.	1.3	772.	−3.7	746.	0.5
r_{36}	708.	(696.) (673.) (664.) (655.)	3.6		718.	1.5	693.	−0.5	720.	0.2	695.	−0.6
r_{37}	631.	(619.)	0.2		634.	0.1	610.	0.1	629.	0.2	613.	0.1
r_{38}	584.	(575.)	−14.9		586.	−13.8	566.	−9.6	586.	−11.2	567.	−10.0
r_{39}	542.	(531.)	0.6		547.	−1.1	527.	−4.9	548.	−3.5	529.	−4.7
r_{49}	416.		−0.1		418.	−0.03	400.	−0.04	416.	−0.02	401.	−0.03
r_{41}	396.		−4.1		395.	−4.3	381.	−4.1	398.	−4.7	382.	−4.0
r_{42}	337.		−7.1		339.	−6.6	328.	−6.6	338.	−6.3	329.	−6.7
r_{43}	194.		7.5		193.	6.1	183.	5.7	191.	8.8	183.	5.5
r_{44}	147.		−3.6		148.	−3.6	144.	−3.0	147.	−3.9	145.	−2.8
r_{45}	59.		26.3		57.	27.3	60.	26.9	60.	25.5	60.	27.1

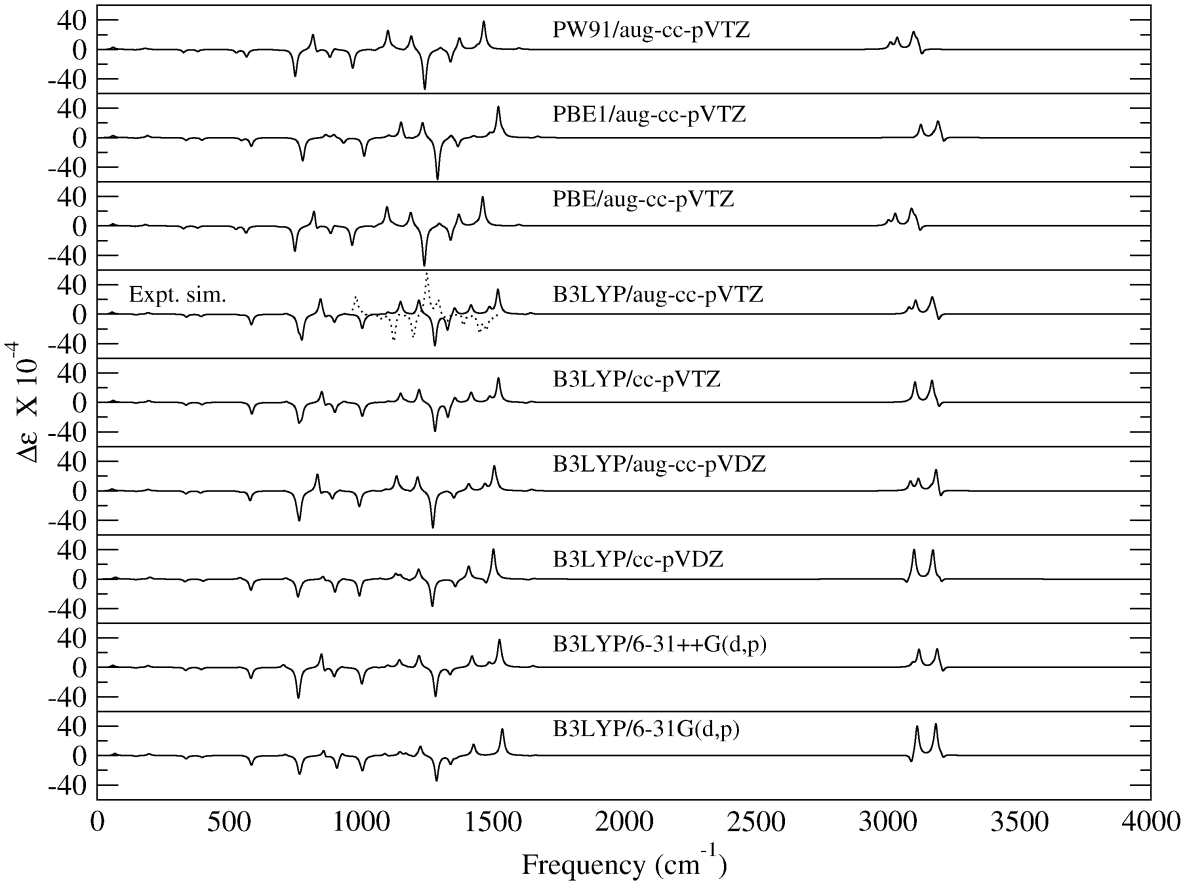

Fig. 3. (R)-Phenyloxirane VCD spectra for various DFT methods.

are presented in Table 3, though there are some regions of the spectra where there are differences. For example, with the 6-31++G(d,p), aug-cc-pVDZ and aug-cc-pVTZ basis sets the lower frequency band in the CH stretch region are both positive, whereas with the basis sets without the diffuse functions, they are of opposite sign. In addition, we also present the calculated vibrational frequencies and rotational strengths at the PBE, PBE1 and PW91 levels of theory with the aug-cc-pVTZ basis set. The spectral simulations for these other DFT methods are also given in Fig. 3. Again we can see the changes with respect to changing the functional are larger than the changes with respect to the basis set at the B3LYP level of theory, but the differences are not that distinct. With the PBE and PW91 functional we also see the positive signed feature in the lower region of the CH stretch region with the aug-cc-pVTZ basis set, similar to what we saw with the basis sets that included the diffuse functions at the B3LYP level.

Hence it appears in order to get the fine features in the VCD spectra, one requires the addition of diffuse functions in addition to the polarization functions, which previously have been shown to be important [72]. Here the basis set dependence clearly affects the VCD intensities more than it has the VA intensities. It appears that larger basis sets are required for calculating VCD intensities at the same level of accuracy as the VA intensities. Therefore, it may be that one might want to increase the quality of the basis set for the calculation if one focuses on VCD intensities in addition to the VA intensities. In many cases, researchers have only focused on the VA intensities of the amide I modes in their determination of the secondary structure content. Keiderling's and Suhai's groups have

shown that the VCD intensities are also very sensitive to secondary structure and can be used in addition to the VA intensities, especially in cases where the VA intensities do not give enough information [80,60,84]. This is not inconsistent with other biomolecular modeling studies where the question one asks or the quantity one wishes to calculate and the accuracy with which one is satisfied determines the method to use (or here basis set for a given method), and not vice versa. In many cases, a method or basis set for a given method will give good results for some quantities, but for other quantities, much larger basis sets for a given method, may be required. A case in point are the dispersion or van der Waals forces of the He_2 dimer, where the binding energy is approximately 11.0 K or 7.65 cm^{-1} experimentally and calculated to be 33.5 μ-Hartrees at the CCSD(T)t-aug-cc-pV6Z counterpoise corrected level of theory [142].

The good agreement between the calculated VA and VCD spectra with the experimental spectra of Ashvar and coworkers [10] leads us to believe that the Raman and ROA spectra will be accurately predicted, given that we have accurate EDEDPD, EDMDPD and ED-EQPD. We give these additional new tests and confirmatory evidence for the accuracy of the geometry and Hessian determined at the DFT level of theory, beyond those reported by Ashvar and coworkers, the predicted Raman scattering and ROA intensities, covered in the next two subsections. Here will also document the accuracy of the B3LYP level of theory with the 6-31G(d,p) and aug-cc-pVDZ basis sets. In addition, we document the accuracy of the RHF level of theory with the 6-31G(d,p) basis set.

3.4. Raman scattering

In Fig. 4 we present our simulated Raman scattering spectra for phenyloxirane. The Raman scattering spectra for phenyloxirane have been reported by Hecht and Barron [64,63]. The Raman intensities monitor changes in the EDEDP as the atoms vibrate. In many cases modes, which are not seen or a very low intensity in the IR or VA spectra, are seen in Raman spectra. For example, the CH stretch mode at 3181 cm^{-1}, that has very little intensity in the VA spectra, has a large intensity in the Raman. Hence the Raman spectral measurements are required to validate the accuracy of this mode, both with respect to the frequency and to its nature in reproducing the Raman intensity, when coupled with the EDEDPD. In addition, the band calculated at 862 cm^{-1} with weak intensity in the VA spectra of Ashvar and coworkers is not observed. The Raman intensity of this band is also calculated to be weak in intensity in our Raman simulations. Hence this band would be hard to see also in the Raman spectra. Surprisingly this band has a calculated strong ROA intensity, so if one could get enough molecules in the path of the laser, then the ROA spectra should be evident, though you might not look for it based the Raman measurements alone.

The agreement between the calculated and measured Raman intensities further gives us a measure of the accuracy of DFT to be able to calculate the EDEDPD. This is important if one wishes to be able to simulate accurately the Raman intensities of the aromatic amino acids, phenylalanine, tryptophan and tyrosine. We have utilized the aug-cc-pVDZ and aug-cc-pVTZ basis sets for our Raman simulations, in addition to the cc-pVDZ and cc-pVTZ basis sets and the 6-31++G(d,p) and the 6-31G(d,p) basis sets. Here we can see that the polarization functions seem to have the largest effects on the Raman spectra, and the additional diffuse functions are not that important as they have been shown to be for van der

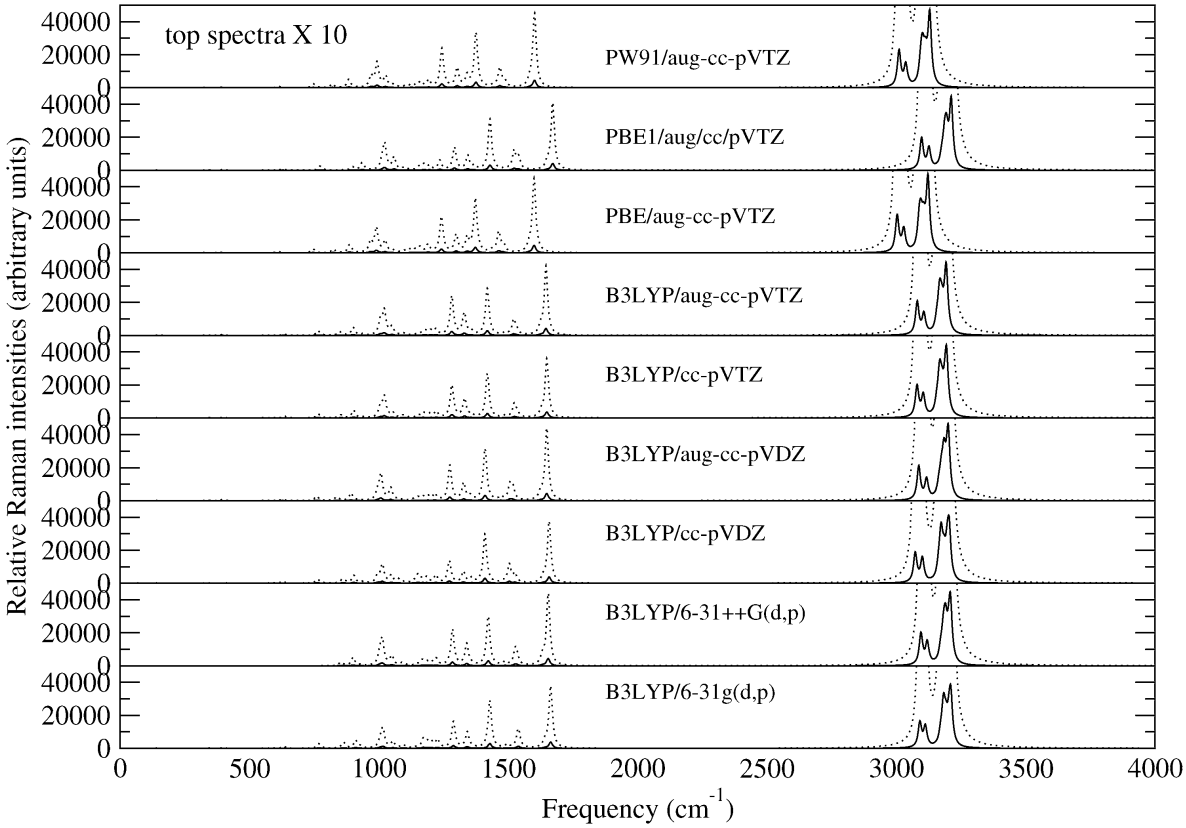

Fig. 4. Phenyloxirane Raman scattering spectra for various DFT methods.

Waals complexes. But to investigate this more thoroughly, we will look to the ROA intensities, discussed in the next subsection. In addition, we have simulated the Raman spectra with the aug-cc-pVTZ basis set at the PBE, PBE1 and PW91 levels. The relative intensities appear to be very similar, but there are some shifts in the frequencies. This is not surprising, given the differences observed in the bond lengths in the oxirane and benzene rings as a function of the DFT functional (method) used. Since the two parent rings, oxirane and benzene, are very symmetrical, the intensities can be to a large extent determined by symmetry and the interactions appear to be such that they are not largely disturbed. In a future work we shall more carefully compare the benzene and oxirane vibrational modes with those found here in phenyloxirane. Since the chirality is reflected in the ROA spectra, it should reveal more information than the simple Raman spectra.

Goddard's group has recently derived new functionals, the XLYP and X3LYP functionals that better treat dispersion than the BLYP and B3LYP functionals [156,155]. These functionals are expected therefore to treat the EDEDP better than the BLYP and B3LYP functionals, but this remains to be shown. The XLYP functional uses the Slater [126], Becke 88 [23] and Perdew 91 [108,111,112] exchange functionals and the Lee, Yang and Parr (LYP) correlation functional [95]. The X3LYP hybrid functional, in addition uses the Hartree–Fock exchange and a bit of the Vosko, Wilk and Nusair (VWN) correlation functional [146]. The testing of these functional for properties, in addition to their testing for geometries and interactions energies remains to be done. In addition, new nonempirical functionals have also recently been developed and implemented in commercial codes [129], which go beyond the GGA approximation and correct some of the deficiencies of the older functionals, for example, the exchange potential's divergence at the nuclei.

In Table 4 we present the calculated vibrational frequencies and Raman scattering intensities (used to simulate the Raman scattering spectra) with the B3LYP hybrid DFT method using the 6-31++G(d,p) and aug-cc-pVTZ basis sets. In addition we present in Fig. 4 the simulated Raman scattering spectra calculated also with the B3LYP hybrid DFT method but with the 6-31G(d,p), cc-pVDZ, aug-cc-pVDZ and cc-pVTZ basis sets. These simulations show that the simulations of the Raman scattering spectra with these basis sets are not drastically different from the two presented here, though the differences are larger visually than those seen at first glance in the VA and VCD spectra. In addition, again we also present the calculated vibrational frequencies and Raman scattering intensities with the PBE, PBE1 and PW91 DFT methods at the highest basis set level we used in this study, that is, the aug-cc-pVTZ. The spectral simulations for these other DFT methods are also given in Fig. 4 and Table 4. Here one sees changes in the peak heights and frequencies that reflect some of the changes in the geometrical parameters (bond lengths and valence angles), which resulted due to changing the DFT exchange correlation functional.

3.5. Raman optical activity

At the B3LYP/6-31++G(d,p) optimized structure we have calculated the Hessian and ED-EDPD that allowed us to simulate the Raman scattering spectra. Additionally, we have calculated the RHF/6-31G(d,p) EDMDPD and EDEQPD, which when combined with the B3LYP/6-31++G(d,p) Hessian and EDEDPD allow us to simulate the ROA spectra. In Fig. 5 we present our DCP and ICP ROA spectra for (R)-phenyloxirane. Comparing our simulated ICP and DCP ROA spectra presented in Fig. 5 with those measured by Hecht and Barron in their works and presented in Figs. 3, 4 and 5 of Ref. [63] and Fig. 4 of Ref. [64], one can see that the main features of the ICP and DCP Raman spectra are reproduced by using the B3LYP/6-31++G** EDEDPD, combined with the RHF/6-31G(d,p) EDMDPD and the EDEQPD.

As one can see in Fig. 4 and in Fig. 5 of Ref. [63] and Fig. 4 of Ref. [64], the low frequency ROA spectra from 0 to 400 cm^{-1} gives additional information about the chirality and stereoisomer of phenyloxirane in a region that is not currently available in VCD measurements. Here we reproduce the $-/+/-/+/-$ sign pattern in the experimental ROA spectra [63]. Hence the ROA and VCD are really complementary in that the low frequency modes are readily measurable in the ROA with currently available ROA instrumentation, while they not with currently available VCD instrumentation.

The low frequency modes are largely collective modes and involve the backbone and side chain modes in proteins. Hence information gained from the Raman and ROA modes will give information about these collective modes. For protein functionality, these modes are very important as in many cases the path the ligand takes to its binding pocket is not obvious from the X-ray structures. Hence information about these collective modes may help to understand the mechanism for protein binding where the binding pockets are buried in crevices, only accessible via collective breathing modes, just those, which are amenable to probing via Raman and ROA spectroscopy.

In addition to the low frequency Raman and ROA spectra of phenyloxirane reported in Ref. [63], the polarized and depolarized Raman and ROA spectra are also reported in the 400 to 1600 cm^{-1} region [64,63]. Here we have information in the same region as we have

Table 4. Comparison of vibrational frequencies and Raman intensities for phenyloxirane

	$\bar{\nu}$ (cm^{-1}) B3LYP ppGdp	($\bar{\nu}$ (cm^{-1})) exp [10]	Ram$_i$ B3LYP ppGdp	$\bar{\nu}$ (cm^{-1}) B3LYP AccpVTZ	Ram$_i$	$\bar{\nu}$ (cm^{-1}) PBE AccpVTZ	Ram$_i$	$\bar{\nu}$ (cm^{-1}) PBE1 AccpVTZ	Ram$_i$	$\bar{\nu}$ (cm^{-1}) PW91 AccpVTZ	Ram$_i$
r_1	3209.		264.5	3193.	292.9	3122.	338.1	3212.	306.6	3129.	335.6
r_2	3203.		70.4	3186.	31.0	3113.	18.4	3204.	13.5	3120.	18.9
r_3	3192.		87.4	3176.	84.2	3105.	107.4	3195.	89.7	3112.	107.0
r_4	3188.		103.1	3169.	95.4	3096.	83.4	3191.	94.8	3103.	81.4
r_5	3181.		103.2	3166.	92.5	3091.	115.3	3185.	83.3	3098.	114.2
r_6	3171.		50.2	3157.	46.1	3086.	48.0	3176.	45.2	3093.	48.9
r_7	3119.		103.9	3106.	95.8	3029.	108.6	3126.	99.4	3036.	106.3
r_8	3095.		151.2	3081.	158.4	3003.	182.6	3098.	151.8	3011.	181.1
r_9	1655.	(1608.) (1601.)	66.0	1646.	63.3	1600	70.0	1672.	60.9	1602.	70.2
r_{10}	1633.	(1586.)	6.8	1625.	6.5	1581.	5.0	1651.	5.7	1582.	5.1
r_{11}	1534.	(1496.)	7.5	1533.	4.2	1482.	7.3	1541.	11.4	1486.	6.5
r_{12}	1527.	(1477.)	13.7	1521.	14.5	1464.	20.7	1523.	18.4	1468.	19.6
r_{13}	1489.	(1452.)	3.5	1489.	2.7	1439.	2.4	1491.	1.6	1443.	2.3
r_{14}	1423.	(1389.) (1383.)	52.5	1419.	49.8	1373.	59.7	1430.	54.1	1375.	60.3
r_{15}	1361.	(1329.) (1311.)	1.1	1357.	4.4	1342.	15.9	1370.	4.3	1342.	12.7
r_{16}	1340.	(1295.) (1288.)	24.2	1330.	24.8	1299.	20.3	1344.	15.9	1303.	22.1
r_{17}	1285.	(1252.)	42.9	1282.	46.3	1242.	43.8	1292.	26.6	1244.	47.4
r_{18}	1222.	(1201.)	8.0	1221.	6.8	1191.	10.0	1236.	11.6	1194.	9.0
r_{19}	1201.	(1177.)	5.1	1200.	5.2	1160.	6.4	1196.	5.2	1163.	6.4
r_{20}	1184.	(1157.)	4.3	1182.	4.1	1144.	4.6	1177.	4.1	1148.	4.6
r_{21}	1168.	(1144.)	6.5	1171.	3.7	1123.	4.4	1171.	4.0	1126.	4.2
r_{22}	1147.	(1126.) (1106.)	4.3	1152.	2.4	1100.	2.4	1154.	4.1	1104.	2.3
r_{23}	1103.	(1077.)	1.0	1104.	0.9	1071.	0.8	1108.	0.9	1073.	0.8

(*continued on next page*)

Table 4. (*Continued*)

	$\bar{\nu}$ (cm^{-1}) B3LYP ppGdp	($\bar{\nu}$ (cm^{-1})) exp [10]	Ram$_i$ B3LYP ppGdp	$\bar{\nu}$ (cm^{-1}) B3LYP AccpVTZ	Ram$_i$	$\bar{\nu}$ (cm^{-1}) PBE AccpVTZ	Ram$_i$	$\bar{\nu}$ (cm^{-1}) PBE1 AccpVTZ	Ram$_i$	$\bar{\nu}$ (cm^{-1}) PW91 AccpVTZ	Ram$_i$
r_{24}	1089.	(1069.)	3.3	1093.	2.4	1051.	3.8	1098.	3.1	1054.	3.5
r_{25}	1050.	(1026.)	13.5	1051.	11.3	1024.	17.0	1059.	17.7	1026.	16.2
r_{26}	1014.	(1002.)	35.3	1021.	34.7	990.	37.5	1023.	34.8	993.	37.8
r_{27}	1006.	(983.)	12.0	1018.	0.2	974.	0.5	1020.	1.5	977.	0.4
r_{28}	1002.		5.0	1006.	21.4	968.	16.4	1014.	11.7	970.	17.0
r_{29}	986.	(966.)	0.1	999.	0.2	955.	0.07	1002.	0.1	958.	0.10
r_{30}	929.	(909.)	1.4	939.	2.1	900.	1.7	941.	2.0	902.	1.7
r_{31}	900.	(877.)	14.0	901.	13.2	887.	13.4	935.	10.7	884.	13.8
r_{32}	862.		0.8	867.	0.9	833.	0.9	898.	5.6	834.	0.6
r_{33}	852.	(819.)	5.9	848.	6.5	824.	6.4	869.	0.6	820.	6.9
r_{34}	767.	(755.)	0.4	778.	0.8	751.	2.7	781.	1.6	752.	2.6
r_{35}	763.	(752.)	9.0	765.	9.0	744.	5.8	772.	7.4	746.	6.1
r_{36}	708.	(696.) (673.) (664.) (655.)	0.0	718.	0.07	693.	0.1	720.	0.1	695.	0.1
r_{37}	631.	(619.)	5.0	634.	3.9	610.	3.7	629.	3.7	613.	3.7
r_{38}	584.	(575.)	1.2	586.	0.9	566.	0.8	586.	0.8	567.	0.8
r_{39}	542.	(531.)	0.5	547.	0.4	527.	0.4	548.	0.3	529.	0.4
r_{49}	416.		0.1	418.	0.1	400.	0.08	416.	0.1	401.	0.1
r_{41}	396.		2.9	395.	3.5	381.	3.9	398.	3.1	382.	3.9
r_{42}	337.		3.0	339.	2.6	328.	2.3	338.	2.2	329.	2.3
r_{43}	194.		0.4	193.	0.6	183.	0.7	191.	0.5	183.	0.7
r_{44}	147.		3.7	148.	3.3	144.	3.3	147.	3.2	145.	3.3
r_{45}	59.		3.2	57.	2.8	60.	3.0	60.	2.8	60.	3.0

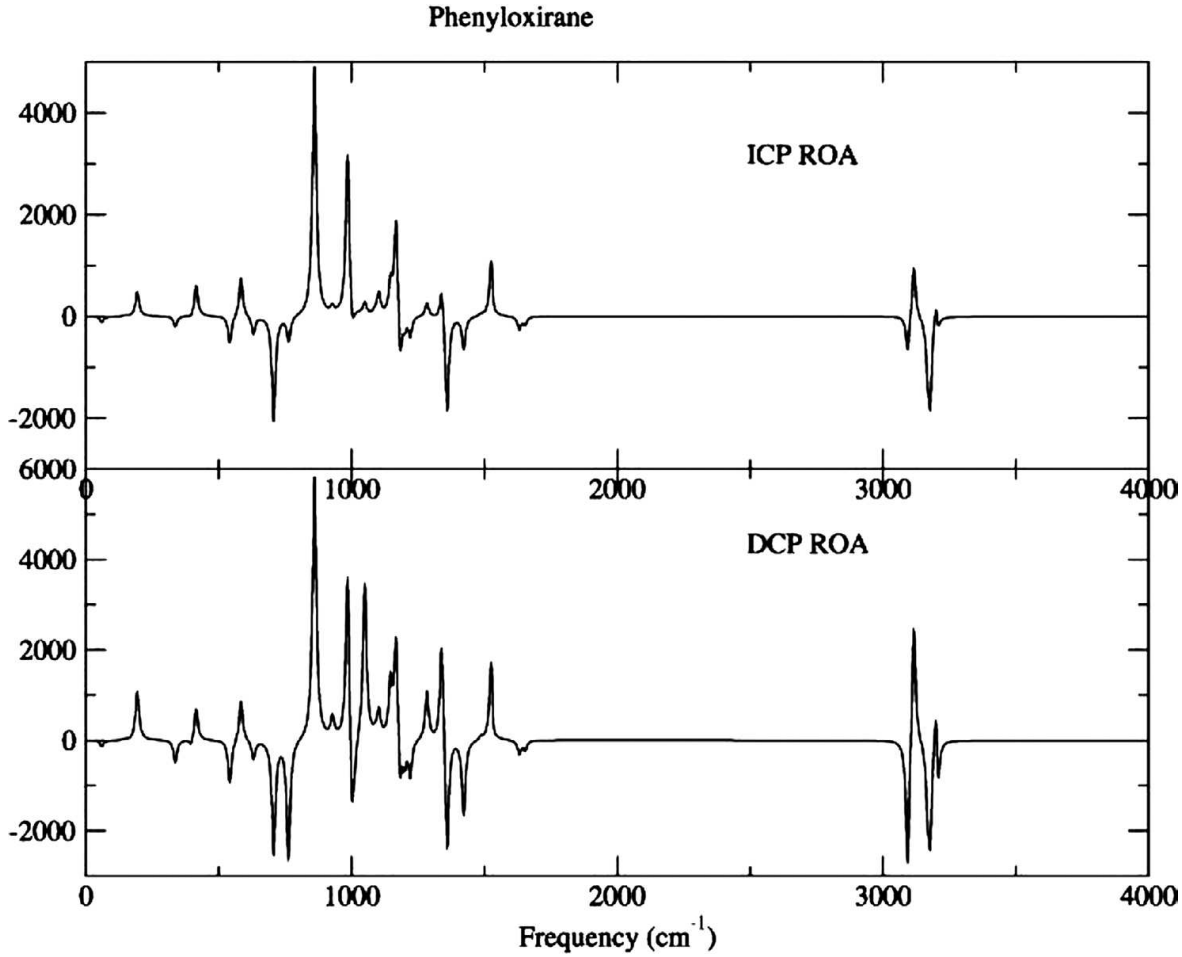

Fig. 5. (R)-Phenyloxirane DCP and ICP Raman optical activity (ROA) spectra calculated with mixed theory (B3LYP/6-31++G(d,p) Hessian and EDEDPD (Gaussian) and RHF/6-31G(d,p) EDMDPD and EDEQPD with CADPAC.

for the VCD. In Figs. 5 and 6 and in Figs. 3 and 4 in Ref. [63] we can compare our predicted with the experimental spectra. In Table 5 we present results utilizing the 6-31G(d,p) basis set, which was used frequently for the early vibrational frequency, Raman scattering, ROA1 (CID1), ROA2 (CID2), ROA3 (CID3), ROA/DCP and ROA/ICP intensity calculations [116,38,60]. Hence we want to document the accuracy of this level of theory also for phenyloxirane. In a future work we will also compare our calculated frequencies, Raman and ROA intensities with the corresponding experimentally measured intensities, which we obtained from trying to integrate the bands in the experimental spectra [37]. It would be nice if the Raman and ROA spectroscopists could report the experimental frequencies, line widths and deconvoluted integrated absolute and relative intensities, similar to the corresponding experimental data reported by the Stephens group for VA and VCD spectra. This makes qualitative comparisons between experiment and theory much easier.

The ROA spectra calculated with the hybrid method (Hessian and EDEDPD at the B3LYP/6-31++G(d,p) level and the EDEQPD and EDMDPD at the RHF/6-31G(d,p) level) are presented in Fig. 5. For large biomolecular structures, the aug-cc-pVDZ basis set might be a comprise between high accuracy and computational cost. A test of this hypothesis can be seen in Fig. 6. In Fig. 6 we present the complete set of spectra (VA, VCD, Raman,

Table 5. Vibrational frequencies, Raman, ROA1 (CID1), ROA2 (CID2), ROA3 (CID3), ROA/DCP and ROA/ICP intensities for (R)-phenyloxirane

	$\bar{\nu}$ (cm^{-1}) B3LYP Gdp	$\bar{\nu}$ (cm^{-1}) B3LYP AcDZ	Ram_i B3LYP Gdp	Ram_i B3LYP AcDZ	$CID1_i$ B3LYP Gdp	CID_i B3LYP AcDZ	$CID2_i$ B3LYP Gdp	$CID2_i$ B3LYP AcDZ	$CID3_i$ B3LYP Gdp	$CID3_i$ B3LYP AcDZ	$\bar{\nu}$ (cm^{-1}) B3LYP ppGdp	Ram_i B3LYP ppGdp	DCP RHF Gdp	ICP RHF Gdp
r_1	3211.	3201.	214.56	286.26	−0.44	−0.14	−0.30	0.09	−2.22	−0.75	3209.	264.5	−11.4	−2.5
r_2	3204.	3195.	94.19	49.26	0.10	0.04	−0.83	−1.06	0.37	0.11	3203.	70.4	11.8	4.3
r_3	3192.	3184.	82.22	114.35	0.20	−0.69	−0.04	−0.52	0.24	−0.80	3192.	87.4	−1.5	−1.2
r_4	3183.	3184.	85.29	68.90	−6.10	−5.14	−2.40	−2.34	−7.99	−8.02	3188.	103.1	4.0	3.0
r_5	3182.	3174.	100.65	97.43	2.25	0.63	0.76	0.28	2.85	0.82	3181.	103.2	−16.9	−13.0
r_6	3172.	3165.	45.07	47.21	1.85	1.10	0.91	0.68	2.70	1.68	3171.	50.4	−10.4	−7.2
r_7	3112.	3117.	97.93	96.60	−1.44	−0.24	−1.62	−0.27	−3.77	−0.66	3119.	103.9	22.5	8.5
r_8	3091.	3087.	120.20	163.23	−0.77	−0.46	−2.82	−2.22	−2.95	−2.18	3095.	151.2	−23.7	−5.9
r_9	1664.	1649.	56.60	66.18	0.95	0.66	0.40	0.34	1.35	0.93	1655.	66.0	−3.1	−2.2
r_{10}	1642.	1626.	5.33	6.24	−0.59	−0.16	−0.46	−0.20	−0.70	−0.19	1633.	6.8	−4.7	−4.0
r_{11}	1542.	1518.	8.16	11.06	3.57	2.88	3.84	3.28	7.45	6.42	1534.	7.5	−9.9	−4.8
r_{12}	1538.	1508.	11.97	14.83	−1.67	0.72	−1.61	0.54	−2.37	1.39	1527.	13.7	33.7	20.7
r_{13}	1497.	1472.	3.48	3.45	26.90	25.56	29.57	27.45	46.49	43.55	1489.	3.5	1.3	0.7
r_{14}	1429.	1411.	50.75	55.64	−0.36	0.11	−1.26	−0.75	−0.85	0.30	1423.	52.5	−28.9	−11.1
r_{15}	1363.	1354.	1.35	4.47	−5.27	−3.73	−1.16	−2.12	−7.58	−8.56	1361.	1.1	−48.9	−35.5
r_{16}	1342.	1328.	17.67	19.35	−4.65	−3.31	−7.20	−6.40	−14.57	−12.45	1340.	24.2	43.9	12.5
r_{17}	1289.	1275.	31.07	41.69	−0.74	0.04	−0.76	0.53	−2.36	0.17	1285.	42.9	20.8	5.4
r_{18}	1227.	1216.	10.39	8.20	−1.33	−4.54	−0.51	−4.75	−1.97	−11.03	1222.	8.0	−16.9	−8.3
r_{19}	1203.	1190.	7.02	5.26	0.96	−0.99	0.51	−0.52	1.53	−2.07	1201.	5.1	−11.5	−5.1
r_{20}	1187.	1171.	6.42	4.33	0.12	0.06	0.10	0.07	0.14	0.07	1184.	4.3	−25.6	−21.8
r_{21}	1172.	1151.	11.22	3.98	1.46	6.88	0.38	2.94	1.73	8.06	1168.	6.5	50.6	43.4
r_{22}	1149.	1136.	1.74	1.98	−9.88	14.40	−11.80	6.99	−14.93	19.91	1147.	1.9	26.4	13.5
r_{23}	1107.	1097.	1.49	0.79	−12.15	−0.98	−3.07	0.73	−14.39	−1.57	1103.	1.0	13.0	9.7
r_{24}	1093.	1077.	4.22	2.61	12.88	7.67	6.50	3.79	18.62	10.52	1089.	3.3	1.9	1.4
r_{25}	1055.	1046.	9.22	17.77	−0.13	−0.09	−0.22	−0.60	−0.65	−1.28	1050.	13.5	81.8	5.4
r_{26}	1016.	1008.	25.44	38.11	−0.02	0.15	0.31	0.78	−0.10	1.63	1014.	35.3	−10.2	−0.9

(*continued on next page*)

Table 5. (*Continued*)

	$\bar{\nu}$ (cm^{-1}) B3LYP Gdp	$\bar{\nu}$ (cm^{-1}) B3LYP AcDZ	Ram$_i$ B3LYP Gdp	Ram$_i$ B3LYP AcDZ	CID1$_i$ B3LYP Gdp	CID$_i$ B3LYP AcDZ	CID2$_i$ B3LYP Gdp	CID2$_i$ B3LYP AcDZ	CID3$_i$ B3LYP Gdp	CID3$_i$ B3LYP AcDZ	$\bar{\nu}$ (cm^{-1}) B3LYP ppGdp	Ram$_i$ B3LYP ppGdp	DCP RHF Gdp	ICP RHF Gdp
r_{27}	1008.	1001.	10.64	0.42	−1.73	9.02	−2.40	9.45	−2.73	12.77	1006.	12.0	−13.2	−4.9
r_{28}	1000.	995.	2.23	11.19	−4.99	−3.94	−7.50	−7.03	−11.36	−10.72	1002.	5.0	−38.2	−8.8
r_{29}	977.	980.	0.13	0.09	45.78	−81.53	43.19	−62.01	166.65	−109.63	986.	0.1	97.9	82.7
r_{30}	929.	921.	2.82	1.74	−5.36	1.87	−0.41	3.69	−7.57	6.13	929.	1.4	11.9	3.3
r_{31}	910.	893.	12.93	12.75	−5.35	−3.58	1.04	0.34	−6.24	−4.33	900.	14.0	−0.2	−0.1
r_{32}	867.	850.	3.73	0.99	−33.79	25.77	−10.60	11.43	−39.61	30.47	862.	0.8	164.1	137.7
r_{33}	862.	837.	7.67	6.65	23.64	7.55	8.31	5.21	27.75	8.81	852.	5.9	15.3	13.1
r_{34}	772.	768.	2.56	1.13	−1.06	4.55	−1.52	10.37	−1.31	16.51	767.	0.4	−7.6	−4.9
r_{35}	766.	760.	7.37	8.72	10.52	6.25	14.55	12.46	44.55	39.64	763.	9.0	−79.4	−12.0
r_{36}	714.	711.	0.58	0.12	−3.27	13.87	−1.38	21.24	−3.96	39.31	708.	0.0	−88.5	−73.2
r_{37}	633.	628.	5.05	4.13	−0.71	−1.06	−0.55	−0.61	−0.84	−1.25	631.	5.0	−16.5	−14.0
r_{38}	586.	581.	1.57	0.91	8.35	1.71	3.97	0.56	9.87	1.99	584.	1.2	39.2	33.5
r_{39}	544.	545.	0.69	0.44	22.51	2.28	15.90	8.33	36.80	5.31	542.	0.5	−44.4	−25.0
r_{40}	418.	415.	0.14	0.07	−129.80	−124.60	−62.21	−98.28	−181.99	−231.09	416.	0.1	43.5	37.1
r_{41}	399.	393.	2.45	3.76	−3.95	−0.92	−2.52	−1.08	−8.98	−2.73	396.	2.9	−10.1	−3.7
r_{42}	338.	337.	3.00	2.56	12.47	7.57	10.38	10.10	23.87	20.84	337.	3.1	−36.6	−15.2
r_{43}	197.	194.	0.29	0.62	−28.36	−9.37	−21.82	−7.17	−63.98	−23.07	194.	0.4	138.6	62.6
r_{44}	148.	149.	5.45	3.40	5.60	5.57	3.35	3.52	6.65	6.65	147.	3.7	3.6	3.0
r_{45}	67.	57.	5.57	2.87	−26.86	−25.99	−11.51	−12.61	−31.49	−30.72	59.	3.2	−58.6	−49.9

Gdp is the 6-31G(d,p) basis set, ppGdp is the 6-31++G(d,p) basis set and AcDZ is the aug-cc-pVDZ basis set.

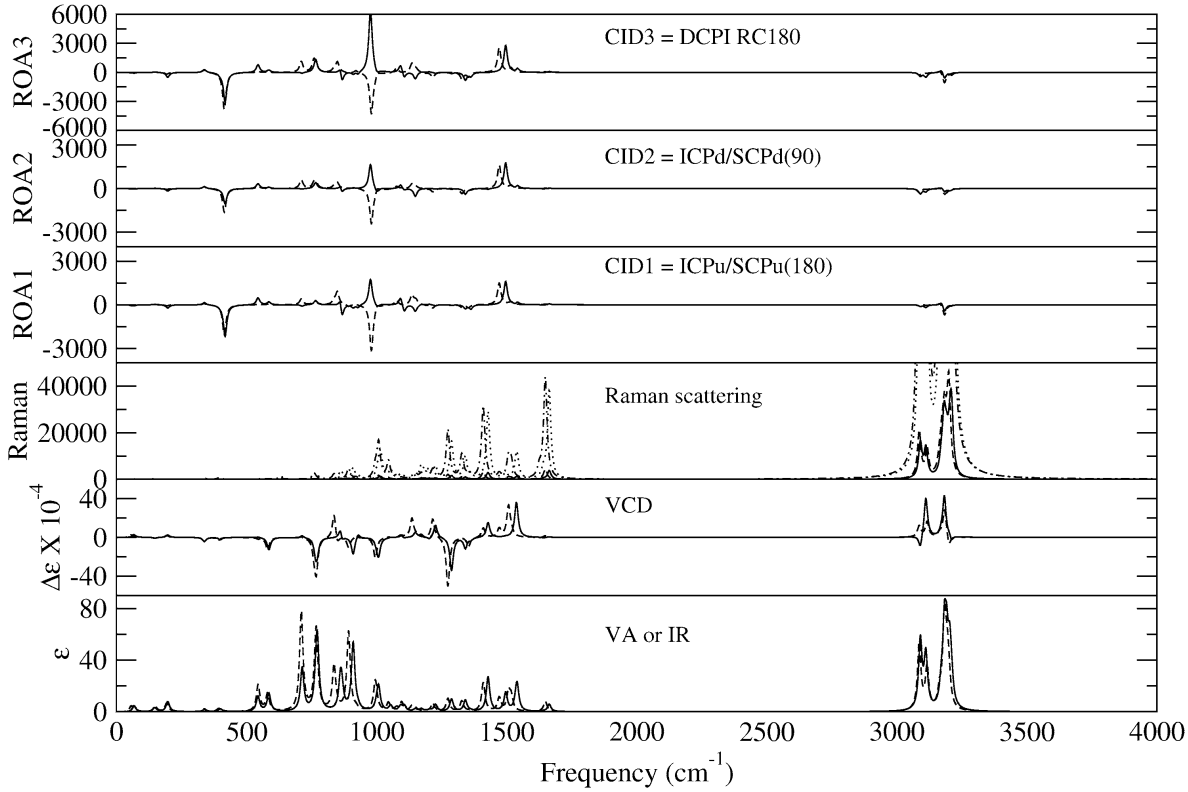

Fig. 6. (R)-Phenyloxirane VA, VCD, Raman, ROA1 (CID1), ROA2 (CID2) and ROA3 (CID3). The solid line spectra calculated at the B3LYP/6-31G(d,p) level (the dotted line is the B3LYP spectra multiplied by 10 for the Raman) and the dashed line at the B3LYP/aug-cc-pVDZ level (the dashed dotted line is the B3LYP/aug-cc-pVDZ spectra multiplied by 10 for the Raman).

ROA1, ROA2 and ROA3) calculated at the B3LYP level of theory with both the 6-31G(d,p) and aug-cc-pVDZ basis sets. Here we see the ROA intensity of the major bands around 980 and 860 cm^{-1} even change in sign when one increases the basis set from 6-31G(d,p) to aug-cc-pVDZ. Here the aug-cc-pVDZ basis set performs much better. This is not unexpected, but shows that the basis set requirements to predict quantitative ROA intensities are higher than those for the Raman intensities. This is similar to the requirement of utilizing a higher quality basis set for VCD spectral intensity calculations than for VA spectral intensity calculations. Hence one is faced with the choice of which basis set one wishes or is required to use for a given spectroscopic property one is interested in, be it just the harmonic frequencies for zero point energy corrections and thermodynamics studies or the VA, VCD, Raman and ROA intensities. If one wishes to have all of these spectra at a relatively high level of accuracy, one is left with the choice of either of the aug-cc-pVDZ or aug-cc-pVTZ basis sets of Dunning. These basis sets appear to the optimal for the combined VA, VCD, Raman and ROA studies.

In Fig. 7 we compare our best combined Raman and ROA spectra, those calculated at the B3LYP/aug-cc-pVDZ level with the experimental Raman and ROA spectra presented by Hecht and Barron [63]. The 6-31G(d,p) basis set is not optimal for calculating the VA, VCD, Raman and ROA spectra. It is a relatively small basis set compared to the complete basis set (CBS) limit, and indeed many people may criticize this basis set as being lacking, but it has been shown to give an adequate accuracy to answer questions in physical

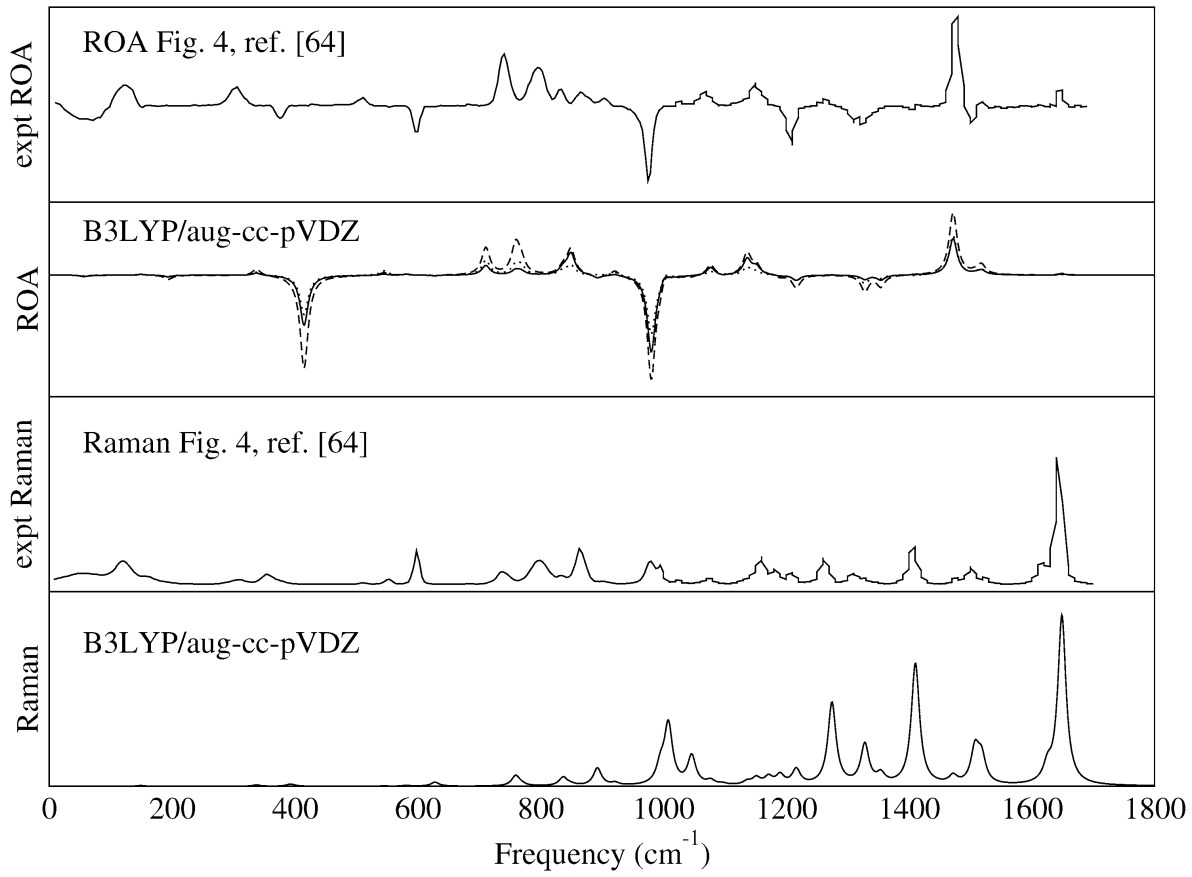

Fig. 7. (R)-Phenyloxirane: Raman spectra for B3LYP/aug-cc-pVDZ; experimental Raman spectra from Hecht *et al.* [64]; ROA1 (CID1), ROA2 (CID2) and ROA3 (CID3) spectra for B3LYP/aug-cc-pVDZ; and experimental ROA spectra from Hecht *et al.* [64].

chemistry, chemical physics, biophysical chemistry and now biophysics by the groups of Polavarapu and Suhai. Hence it is worthwhile to document its accuracy, both quantitatively and visually in comparison to larger basis sets, for example, the aug-cc-pVDZ basis set, which give more accurate values, both for DFT and *ab initio* methods.

The agreement with the experimental data, as extracted from the spectra as anharmonic vibrational frequencies, dipole strengths, rotational strengths and relative integrated peaks in the Raman and ROA experiments is very good with the aug-cc-pVDZ basis set. It increases, however, when one goes to the aug-cc-pVTZ basis set that is seen in Fig. 7 where we compare the Raman and ROA spectra with the experimental Raman and ROA spectra [64] and in Fig. 8 where we compare the VA and VCD spectra with the experimental VA and VCD spectra [10]. The 6-31G(d,p) gives qualitative good results, but can be improved significantly by going to either the aug-cc-pVDZ or aug-cc-pVTZ basis sets. We have only documented the aug-cc-pVTZ basis set for the VA, VCD and Raman spectra. In the future we will also present the ROA spectra for phenyloxirane with the aug-cc-pVTZ basis set and hence document this basis set for reproducing the experimental ROA spectra. But the agreement to date with the aug-cc-pVDZ basis set is excellent, so it should only get better and give us semi-quantitative accuracy of the intensities. To date only the general features in the ROA spectra have been reproduced, which has allowed for stereoisomerical and conformational studies to be undertaken. With higher accuracy calculations and interpre-

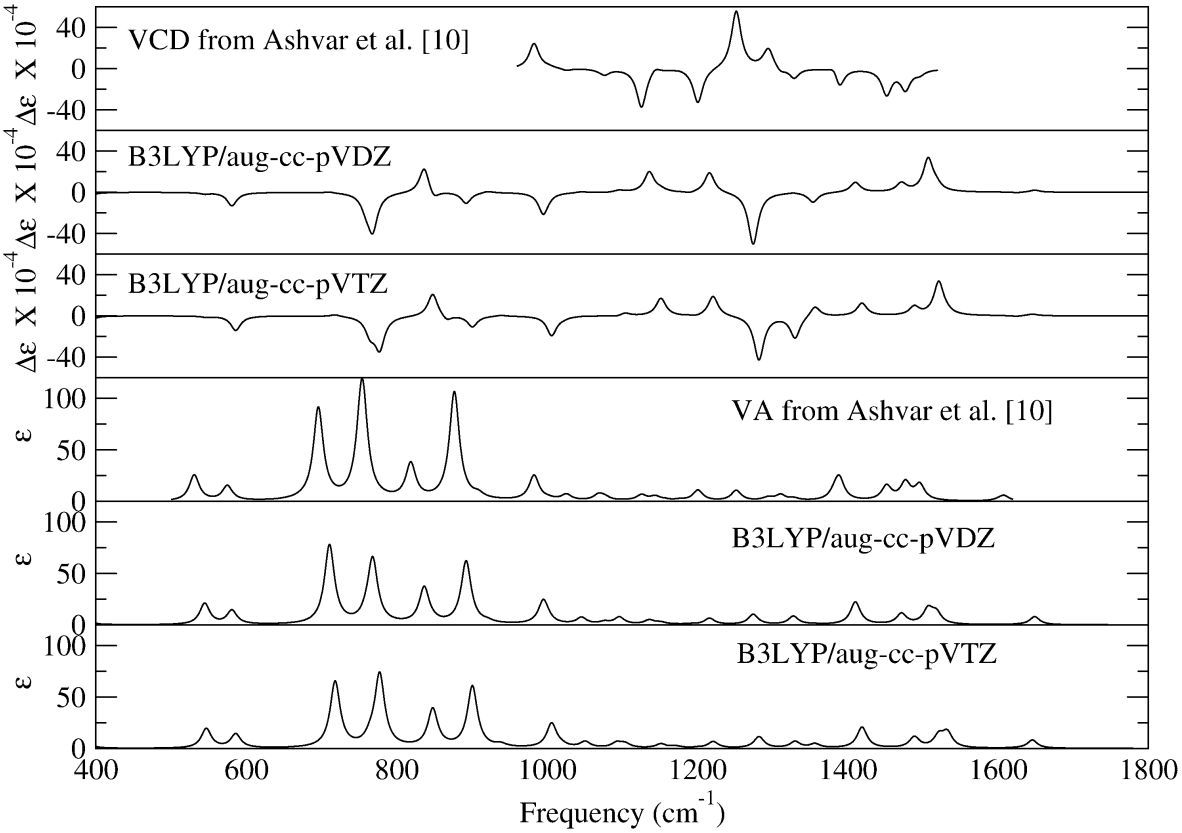

Fig. 8. (R)-Phenyloxirane (RPO): VA spectra for RPO at B3LYP/aug-cc-pVTZ level; VA spectra for RPO at B3LYP/aug-cc-pVDZ level; experimental VA spectra for (S)-Phenyloxirane (SPO) from Ashvar *et al.* [10]; VCD spectra for RPO at B3LYP/aug-cc-pVTZ level; VCD spectra for RPO at B3LYP/aug-cc-pVDZ level; and experimental VCD spectra for SPO from Ashvar *et al.* [10].

tations of Raman and ROA spectra now feasible, more quantitative and detailed questions can hopefully be answered.

Finally in Fig. 7 we compare our B3LYP/aug-cc-pVDZ Raman and ROA simulations with the experimental Raman and ROA spectra extracted from Fig. 4 in Hecht *et al.* [64]. The agreement between the calculated and measured spectra is excellent and the best that we have reported to date. Here we have used the B3LYP level of theory, which Stephens has used and found to give good agreement with the VA and VCD spectra, though with a slightly different basis set.

The aug-cc-pVDZ basis set appears to be able to well reproduce the Raman and ROA spectra, much better than the smaller 6-31G(d,p) that we and other groups have previously used. Finally in Fig. 8 we compare our VA and VCD spectra calculated at the B3LYP/aug-cc-pVXZ, X = D and T, levels with the experimental VA and VCD spectra [10]. Again we see remarkable agreement. These combinations appear to be the best to date and we look forward to further documenting their performance for systems where there has been shown to be strong interactions between the solvent and solute. Previously we did not get optimal agreement in such systems and this may have been due to our use of the relatively small 6-31G(d,p) basis set and the RHF EDMDPD and EDEQPD [60,74,75]. We look forward to reexamining these systems now with the more accurate EDMDPD and EDEQPD. Ad-

ditionally we should look at the effects due to temperature and frequency of the laser used in the Raman and ROA experiments.

The EDMDPD and EDEQPD have not yet been implemented at the XLYP and X3LYP levels of theory, though Stephens and coworkers and recently implemented the EDMDP at the BLYP and B3LYP levels in a development version of Gaussian. These new features are now available in Gaussian 2003 RevC.02, which we have used for our new DFT ROA simulations. In addition, Ruud and Helgaker have recently implemented these tensors at the DFT level in a development version of the Dalton program [119]. We are also in the progress of implementing these tensors using an alternative formulation in a development version of CADPAC. In addition, the XLYP and X3LYP functionals are being implemented as they appear to be the best available functionals for modeling biomolecules, where both H-bonding and dispersion forces are important. In addition, other new functionals must continually be added, especially those which treat van der Waals (dispersion) forces more accurately, charge transfer effects and finally excited electronic states [39,32,128,120,90, 91,55,82,141,107,17,140,45,56,143,96,113,88,147,100,7,8,102]. There has been some recent discussion on how to adequately treat all of these effects self consistently, but to date there is no general consensus in the different communities [101,58,158,157,144,152,25, 153,135,121,42,70,154,41,31,49,40,71,118].

The EDMDP tensors have also been used to calculate the optical rotation spectra [29,13,59]. In addition, recently solvent effects have also been taken into effect via a continuum model [103]. Hence this is a good start in the continuum solvent approach to optical rotation spectra, which can also be applied to ROA simulations.

Alternative formulation of the EDMDP tensors utilizing current density functional theory [93,34,94,92,145] as an alternative to the recently implemented formulation by Stephens, Frisch and Cheeseman [29] and Bak, Rudd, Jørgensen, Olsen and Helgaker [67,119] would be similar to the alternative formulations of the AAT. In addition, the newly derived functionals that treat dispersion and H-bonding better than the BLYP and B3LYP are also expected to better Raman and ROA intensities. In addition, the dynamic polarizabilities, which can be calculated by TD-DFT should also improve the accuracy, especially as one approaches an electronic transition, where the static limit should no longer be valid. It is surprising how good the agreement has been using the simple static limit for the ED-EDPD, EDMDPD and EDEQPD. We are presently investigating the frequency dependence of the ROA spectra as a function of the exciting laser wavelength, both far from resonance with electronic transitions, then near resonance and finally resonance ROA. This has applications for the near or resonance enhanced Raman and ROA for aromatic amino acids, phenylalanine, tryptophan and tyrosine. It would be nice to take into account the interaction with surfaces, as the phenomenon of surface enhanced Raman scattering and the analogous phenomenon surfaced enhanced Raman optical activity are areas of interest in our group. Here modeling studies could greatly add to the physical understanding of these phenomenon. To date, the interpretation of the spectra and spectral changes have limited the application of these phenomenon.

These four vibrational spectroscopies, VA, VCD, Raman and ROA, have now reached the stage experimentally and theoretically where they can all be measured routinely in the spectroscopy laboratory and simulated in the quantum theory laboratory. These spectroscopies now can be used along with NMR and X-ray crystallography to answer questions and pose new experiments that should greatly add to our understanding.

4. DISCUSSION

To make measurements on individual molecules requires specialized experimental techniques able to measure the response of either individual or small numbers of molecules. The microwave, infrared or vibrational absorption, and Raman spectra of molecules in the gas phase are the two most common techniques to get structural and functional group information. Another technique is to isolate the molecules in an inert low temperature matrix, for example, Ar or N_2, to perform VA, VCD, Raman, ROA, UV-Vis, ECD, and EPR spectra [125]. Here one is interested in understanding the properties of the individual molecules and also the forces responsible for the stabilization of the low energy conformers. Such data are invaluable to theoreticians who want to benchmark their levels of theory. The bond lengths, valence angles, torsional angles and dipole moments can be determined from microwave studies. From the VA, VCD, Raman and ROA spectra one can get the vibrational frequencies and information about how the electric dipole, magnetic dipole, the EDEDP, the EDMDP, and the EDEQP change with changes in nuclear coordinates. The problem is that normally one does not have enough experimental data to completely determine these quantities. Hence theoretical models are needed to even interpret the experimental data measured, hence the real synergistic relationship between theory and experiment.

From the ECD, VCD and ROA spectra we can get information on the chirality of a molecule [65]. For a molecule with conformational flexibility, one can get conformational data. In addition to gas phase and low temperature matrix measurements, one can in many cases also make measurements on molecules in nonpolar solvents or embedded in micelles. If one can overcome the problem of solubility one can also make measurements of the VA, VCD, Raman, ROA, NMR, EPR, UV-Vis and ECD spectra of molecules. The information is the same for the gas phase as for a low temperature matrix, but the line widths of the spectral features can broaden, so one has in many cases an assignment and deconvolution problem. Here one is aided by theoretical calculations of the spectra for these molecules. In all of the above cases the spectral simulations are relatively straightforward as one must not in general treat the environment explicitly. The assumption is that the nonpolar environment or inert matrix does not greatly perturb the molecule and therefore its properties, or at least one assumes that it does not.

5. CONCLUSIONS AND FUTURE PERSPECTIVES

In this work we have attempted to use the current developments in quantum chemistry to interpret the Raman and ROA spectra of phenyloxirane, one of the first measurements made with right-angle scattering ROA. At the time of these measurement in 1994, the size of the molecule did not allow for a complete high level density functional analysis. With the recent developments in quantum chemistry by the groups developing CADPAC (R.D. Amos, J. Rice, D.J. Tozer and N. Handy), Gaussian (Michael Frisch and J.R. Cheeseman) and Dalton (K. Bak, P. Jørgensen, T. Helgaker, J. Olson and K. Rudd), the interpretation of the VA, VCD, Raman and ROA spectra can now be routinely calculated. With the availability of FTIR VCD instruments by Thermo Electron, Bruker and Bomen and Raman and ROA by Biotools, these spectroscopies can now be used to routinely answer structural and functional groups questions on systems where X-ray crystallography and NMR have not been

able to. In addition, the fast time scale for these spectroscopies allows us to make measurements that are the superposition of the components and not the average. The possible applications for these spectroscopies lie only within the imaginations of the groups working in the field. Future developments that are required are the analytical implementation of the EDMDPD and EDEQPD at the DFT level with a linear scaling algorithm, similar to the currently implemented methods by the SIESTA and SCC-DFTB developed in Barcelona and Heidelberg/Paderborn/Georgia [117,150,149,46,47,61,27,48,44,50,122,106].

In addition, the treatment of the solvent has recently been shown to be very important in stabilizing the zwitterionic species of L-alanine [137] and L-alanyl-alanine [87] and in also producing a conformer for NALANMA that is not found in the gas phase (isolated state) or by using continuum models [80,38,60]. Hence the treatment of explicit solvent water molecules that are directly H-bonded with the polar groups of proteins and, which stabilize the charge via solvation on charged species must be taken into account. Therefore, the determination of the structure and at the optimized structure of the complex, the Hessian is a more difficult problem than originally thought.

The treatment of the second hydration shell and bulk water can probably be treated with the continuum models, so this work was and is by no means not important and unnecessary. On the contrary it is very important and hybrid solvent models may become the best way to treat the solvent effects as do the hybrid exchange correlations functional seem to be the best way at present to treat dispersion effects, H-bonding and the hydrophobic effects (other weak interactions) that have not been adequately treated.

In addition, charge transfer effects may also be important and the recently developed CAM-LYP and CAM-3LYP density functional may be they way we treat these charge transfer effects until more refined methods are developed [158]. In addition, if one wishes to take temperature into account, the QM/MM-MD method can be used. Here as the linear scaling methods are extended so that all of the properties can be calculated at each step of the MD run, then one can foresee being able to simulate the VA, VCD, Raman and ROA spectra by doing the required time to frequency transformations. One will automatically get the required anharmonic effects, which are currently missing in addition to the effects of temperature. It is very important to treat the solvent in an accurate way, which means simple charge models for the first solvation shell waters will not be accurate enough as they will miss the directionality present in H-bonding as shown by the group of Buckingham. The lone pairs have been shown to be very important to get the tetrahedral H-bonding structure. So the present state of quantum chemistry is undergoing a revival with respect to explicit solvent treatment. Here the simple basis set superposition error (BSSE) treatment of dimers and trimers will be exacerbated by having to treat many more water molecules in the molecular complexes. Here there is also plenty of room for new methods and new ways to accurately calculate binding energies, solvation energies and free energies, the hydrophobic effect and even the dynamic structures that are present in the various experiments, be they vibrational, NMR, EPR or X-ray or neutron or electron diffraction measurements. The need for quantum chemists to be able to help interpret the wealth of new and interesting experimental data was never so needed and so fruitful.

ACKNOWLEDGEMENTS

KJJ would like to thank the Danish National Research Foundation and the Quantum Protein (QuP) Center for his salary as an associate professor (lector) at QuP during the 5 year

funding period of QuP (2001–2006). In addition, we would like to thank Prof. Nick Handy and Roger D. Amos for providing a copy of CADPAC, which allows one to calculate the required tensors to simulate the ROA spectra. VWJ would like to thank the Danish National Research Foundation and QuP for her PhD scholarship. Finally we would like to thank the kind referee of the first version of this manuscript for his/her many thoughtful and critical comments, which have helped us make this a much nicer manuscript.

REFERENCES

[1] R.D. Amos, *Chem. Phys. Lett.* **87** (1982) 23.
[2] R.D. Amos, *Chem. Phys. Lett.* **108** (1984) 185.
[3] R.D. Amos, *Chem. Phys. Lett.* **124** (1986) 376.
[4] R.D. Amos, N.C. Handy, K.J. Jalkanen, P.J. Stephens, *Chem. Phys. Lett.* **133** (1987) 21.
[5] R.D. Amos, K.J. Jalkanen, P.J. Stephens, *J. Phys. Chem.* **92** (1988) 5571.
[6] R.D. Amos, J.E. Rice, *Cambridge Analytical Derivatives Package (CADPAC)*, 5.2 edition, Cambridge Univ. Press, Cambridge, UK, 1994.
[7] Y. Andersson, E. Hult, P. Apell, D.C. Langreth, B.I. Lundqvist, *Solid State Comm.* **106** (1998) 235.
[8] Y. Andersson, D.C. Langreth, B.I. Lundqvist, *Phys. Rev. Lett.* **76** (1996) 102.
[9] C.S. Ashvar, F.J. Devlin, K.L. Bak, P.R. Taylor, P.J. Stephens, *J. Phys. Chem.* **100** (1996) 9262.
[10] C.S. Ashvar, F.J. Devlin, P.J. Stephens, *J. Am. Chem. Soc.* **121** (1999) 2836.
[11] C.S. Ashvar, F.J. Devlin, P.J. Stephens, K.L. Bak, T. Eggimann, H. Wieser, *J. Phys. Chem. A* **102** (1998) 6842.
[12] C.S. Ashvar, P.J. Stephens, T. Eggimann, H. Wieser, *Tetrahedron: Asymmetry* **9** (1998) 1107.
[13] J. Autschbach, S. Patchkovskii, T. Ziegler, S.J.A. van Gisbergen, E.J. Baerends, *J. Chem. Phys.* **117** (2002) 581.
[14] K.L. Bak, F.J. Devlin, C.S. Ashvar, P.R. Taylor, M.J. Frisch, P.J. Stephens, *J. Phys. Chem.* **99** (1995) 14918.
[15] K.L. Bak, P. Jørgensen, T. Helgaker, K. Ruud, H.J.Aa. Jensen, *J. Chem. Phys.* **98** (1993) 8873.
[16] K.L. Bak, P. Jørgensen, T. Helgaker, K. Ruud, H.J.Aa. Jensen, *J. Chem. Phys.* **100** (1994) 6621.
[17] A. Banerjee, M.K. Karbola, *J. Chem. Phys.* **117** (2002) 7845.
[18] L.D. Barron, M.P. Bogaard, A.D. Buckingham, *J. Am. Chem. Soc.* **95** (1973) 603.
[19] L.D. Barron, A.D. Buckingham, *Mol. Phys.* **20** (1971) 1111.
[20] L.D. Barron, A.D. Buckingham, *Annu. Rev. Phys. Chem.* **26** (1975) 381.
[21] L.D. Barron, A.R. Gargaro, L. Hecht, P.L. Polavarapu, *Spectrochim Acta A* **47** (1991) 1001.
[22] L.D. Barron, L. Hecht, E.W. Blanch, A.F. Bell, *Progr. Biophys. Molecular Biol.* **117** (2000) 1.
[23] A.D. Becke, *Phys. Rev. A* **38** (1988) 3098.
[24] A.D. Becke, *J. Chem. Phys.* **104** (1996) 1040.
[25] A.D. Becke, *J. Chem. Phys.* **119** (2003) 2972.
[26] H. Berman, K. Henrick, H. Nakamura, *Nature Structural Biol.* **10** (2003) 980.
[27] H.G. Bohr, K.J. Jalkanen, K. Frimand, M. Elstner, S. Suhai, *Chem. Phys.* **246** (1999) 13.
[28] A.D. Buckingham, P.W. Fowler, P.A. Galwas, *Chem. Phys.* **112** (1987) 1.
[29] J.R. Cheeseman, M.J. Frisch, F.J. Devlin, P.J. Stephens, *J. Phys. Chem. A* **104** (2000) 1039.
[30] J.R. Cheeseman, M.J. Frisch, F.J. Devlin, P.J. Stephens, *Chem. Phys. Lett.* **252** (1996) 211.
[31] T.C. Choy, *Phys. Rev. A* **62** (2000) 012506.
[32] X. Chu, A. Dalgarno, *J. Chem. Phys.* **121** (2004) 4083.
[33] T. Clark, J. Chandrasekhar, G.W. Spitznagel, P.v.R. Schleyer, *J. Comp. Chem.* **4** (1983) 294.
[34] S.M. Colwell, N.C. Handy, A.M. Lee, *Phys. Rev. A* **53** (1996) 1316.
[35] D.P. Craig, T. Thirunamachandran, *Mol. Phys.* **35** (1978) 825.
[36] M.P. de Lara-Castells, R.V. Krems, A.A. Buchachenko, G. Delgado-Barrio, P. Villarreal, *J. Chem. Phys.* **115** (2001) 10438.
[37] I.M. Degtyarenko, PhD thesis, Helsinki University of Technology, 2006 expected.
[38] Z. Deng, P.L. Polavarapu, S.J. Ford, L. Hecht, L.D. Barron, C.S. Ewig, K.J. Jalkanen, *J. Phys. Chem.* **100** (1996) 2025.
[39] M. Dion, H. Rydberg, E. Schroeder, D.C. Langreth, B.I. Lundqvist, *Phys. Rev. L* **92** (2004) 246401.

[40] J.F. Dobson, J. Wang, *Phys. Rev. Lett.* **82** (1999) 2123.
[41] J.F. Dobson, J. Wang, *Phys. Rev. B* **62** (2000) 10038.
[42] J.F. Dobson, J. Wang, T. Gould, *Phys. Rev. B* **66** (2002) 081108.
[43] T.H. Dunning Jr., *J. Chem. Phys.* **90** (1989) 1007.
[44] M. Elstner, Weiterentwichlung quantenmechanischer Rechenverfahren fuer organische Molekuele und Polymere, Ph.D. thesis, Universitaet-Gesamthochschule Paderborn, Paderborn, Deutschland, April 1998.
[45] M. Elstner, P. Hobza, S. Suhai, E. Kaxiras, *J. Chem. Phys.* **114** (2001) 5149.
[46] M. Elstner, K.J. Jalkanen, M. Knapp-Mohammady, Th. Frauenheim, S. Suhai, *Chem. Phys.* **263** (2001) 203.
[47] M. Elstner, K.J. Jalkanen, M. Knapp-Mohammady, Th. Frauenheim, S. Suhai, *Chem. Phys.* **256** (2000) 15.
[48] M. Elstner, D. Porezag, G. Jungnickel, J. Elsner, M. Haugk, Th. Frauenheim, S. Suhai, G. Seifert, *Phys. Rev. B* **58** (1998) 7260.
[49] E. Engel, A. Höck, R.M. Dreizler, *Phys. Rev. A* **61** (2000) 032502.
[50] M.V. Fernandex-Serra, J. Junquera, C. Jelsch, E. Artacho, *Solid State Comm.* **16** (2000) 395.
[51] K. Frimand, K.J. Jalkanen, *Chem. Phys.* **279** (2002) 161.
[52] K. Frimand, K.J. Jalkanen, H.G. Bohr, S. Suhai, *Chem. Phys.* **255** (2000) 165.
[53] M.J. Frisch, J.A. Pople, J.S. Binkley, *J. Chem. Phys.* **80** (1984) 3265.
[54] M.J. Frisch, G.W. Trucks, H.B. Schlegel, G.E. Scuseria, M.A. Robb, J.R. Cheeseman, J.A. Pople, *Gaussian 03, Revision C.02*, Gaussian Inc., Pittsburg, PA 15106, 2003.
[55] M. Fuchs, X. Gonze, *Phys. Rev. B* **65** (2002) 235109.
[56] A. Goerling, H.H. Heinze, M. Levy, *J. Mol. Struct. (Theochem)* **501–502** (2000) 271.
[57] L.A. Gribov, W.J. Orville-Thomas, Theory of intensities in the Raman spectra of polyatomic molecules, in: *Theory and Methods of Calculation of Molecular Spectra*, John Wiley and Sons, New York, 1988, pp. 563–595.
[58] S. Grimme, *J. Comput. Chem.* **25** (2004) 1463.
[59] S. Grimme, F. Furche, R. Ahlrichs, *Chem. Phys. Lett.* **361** (2002) 321.
[60] W.-G. Han, K.J. Jalkanen, M. Elstner, S. Suhai, *J. Phys. Chem. B* **102** (1998) 2587.
[61] W.-G. Han, M. Elstner, K.J. Jalkanen, Th. Frauenheim, S. Suhai, *Int. J. Quantum Chem.* **78** (2000) 459.
[62] A.E. Hansen, P.J. Stephens, T.D. Bouman, *J. Phys. Chem.* **95** (1991) 4255.
[63] L. Hecht, L.D. Barron, J. Raman, *Spectrosc.* **25** (1994) 443.
[64] L. Hecht, L.D. Barron, *J. Mol. Struct.* **347** (1995) 449.
[65] L. Hecht, A.L. Phillips, L.D. Barron, *J. Raman Spectrosc.* **26** (1995) 727.
[66] W.J. Hehre, R. Ditchfield, J.A. Pople, *J. Chem. Phys.* **56** (1972) 2257.
[67] T. Helgaker, K. Ruud, K.L. Bak, P. Jørgensen, J. Olsen, *Faraday Discuss.* **99** (1994) 165.
[68] G. Holzwarth, E.C. Hsu, H.S. Mosher, T.R. Faulkner, A. Moscowitz, *J. Am. Chem. Soc.* **96** (1974) 251.
[69] E.C. Hsu, G. Holzwarth, *J. Chem. Phys.* **59** (1973) 4678.
[70] E. Hult, P. Hyldgaard, J. Rossmeisl, B.I. Lundqvist, *Phys. Rev. B* **64** (2001) 195414.
[71] E. Hult, H. Rydberg, B.I. Lundqvist, *Phys. Rev. B* **59** (1999) 4708.
[72] K.J. Jalkanen, Vibrational absorption, vibrational circular dichroism and magnetic susceptibilities, Ph.D. thesis, University of Southern California, Los Angeles, CA, USA, 1989.
[73] K.J. Jalkanen, M. Elstner, S. Suhai, *J. Mol. Struct. (Theochem)* **675** (2004) 61.
[74] K.J. Jalkanen, R.M. Nieminen, K. Frimand, J. Bohr, H.G. Bohr, R.C. Wade, E. Tajkhorshid, S. Suhai, *Chem. Phys.* **265** (2001) 125.
[75] K.J. Jalkanen, R.M. Nieminen, M. Knapp-Mohammady, S. Suhai, *Int. J. Quantum Chem.* **92** (2003) 239.
[76] K.J. Jalkanen, P.J. Stephens, *J. Phys. Chem.* **95** (1991) 5446.
[77] K.J. Jalkanen, P.J. Stephens, R.D. Amos, N.C. Handy, *Chem. Phys. Lett.* **142** (1987) 153.
[78] K.J. Jalkanen, P.J. Stephens, R.D. Amos, N.C. Handy, *J. Phys. Chem.* **92** (1988) 1781.
[79] K.J. Jalkanen, P.J. Stephens, P. Lazzeretti, R. Zanasi, *J. Chem. Phys.* **90** (1988) 3204.
[80] K.J. Jalkanen, S. Suhai, *Chem. Phys.* **208** (1996) 81.
[81] B.G. Johnson, J. Florian, *Chem. Phys. Lett.* **247** (1995) 120.
[82] M. Kamiya, T. Tsuneda, K. Hirao, *J. Chem. Phys.* **117** (2002) 6010.
[83] R.W. Kawiecki, F.J. Devlin, P.J. Stephens, R.D. Amos, *J. Phys. Chem.* **95** (1991) 9817.
[84] T.A. Keiderling, Protein structural studies using vibrational circular dichroism spectroscopy, in: *Spectroscopic Methods For Determining Protein Structure in Solution*, VCH Publishers Inc., 69451 Weinheim, Germany, 1996, pp. 163–189.
[85] T.A. Keiderling, *Curr. Opin. Chem. Biol.* **6** (2002) 682.

[86] R.A. Kendall, T.H. Dunning Jr., R.J. Harrison, *J. Chem. Phys.* **96** (1992) 6796.
[87] M. Knapp-Mohammady, K.J. Jalkanen, F. Nardi, R.C. Wade, S. Suhai, *Chem. Phys.* **240** (1999) 63.
[88] W. Kohn, Y. Meir, D.E. Makarov, *Phys. Rev. Lett.* **80** (1998) 4153.
[89] A. Komornicki, J.W. McIver, *J. Chem. Phys.* **70** (1979) 2014.
[90] N. Kurita, H. Inoue, H. Sekino, *Chem. Phys. Lett.* **370** (2003) 161.
[91] N. Kurita, H. Sekino, *Int. J. Quantum Chem.* **91** (2003) 355.
[92] A.M. Lee, S.M. Colwell, N.C. Handy, *Chem. Phys. Lett.* **229** (1994) 225.
[93] A.M. Lee, N.C. Handy, *Phys. Rev. A* **59** (1999) 209.
[94] A.M. Lee, N.C. Handy, S.M. Colwell, *J. Chem. Phys.* **103** (1995) 10095.
[95] C. Lee, W. Yang, R.G. Parr, *Phys. Rev. B* **37** (1988) 785.
[96] M. Lein, J.F. Dobson, E.K.U. Gross, *J. Comp. Chem.* **20** (1999) 12.
[97] D.A. Long, *Raman Spectroscopy*, McGraw-Hill, New York, 1977.
[98] R.C. Lord, *Appl. Spectrosc.* **31** (1977) 187.
[99] O. Lund, K. Frimand, J. Gorodkin, H.G. Bohr, J. Bohr, J. Hansen, S. Brunak, *Protein Eng.* **10** (1997) 1241.
[100] B.I. Lundqvist, E. Hult, H. Rydberg, A. Bogicevic, J. Strömquist, D.C. Langreth, *Progr. Surf. Sci.* **59** (1998) 149.
[101] R.J. Magyar, A. Fleszar, E.K.U. Gross, *Phys. Rev. B* **69** (2004) 045111.
[102] F. Mele, T. Mineva, N. Russo, M. Toscano, *Theor. Chim Acta* **91** (1995) 169.
[103] R. Mennucci, J. Tomasi, R. Cammi, J.R. Cheeseman, M.J. Frisch, F.J. Devlin, S. Gabriel, P.J. Stephens, *J. Phys. Chem. A* **106** (2002) 6102.
[104] M.G. Mulkerrin, Protein structure analysis using circular dichroism, in: *Spectroscopic Methods for Proteins in Solution*, VCH Publishers Inc., 69451 Weinheim, Germany, 1996, pp. 5–27.
[105] P. Ordejon, E. Artacho, J.M. Soler, *Phys. Rev. B (Rapid Comm.)* **53** (1996) R10441.
[106] P. Ordejon, E. Artacho, J.M. Soler, The SIESTA method for linear scaling *ab initio* simulations, *PHI-K Newsletter* **53** (1996) 134.
[107] M.D. Patey, C.E.H. Dessent, *J. Phys. Chem. A* **106** (2002) 4623.
[108] J.P. Perdew, *Electronic Structure Theory of Solids*, Akademie Verlag, Berlin, 1991, p. 11.
[109] J.P. Perdew, K. Burke, M. Ernyerhoh, *Phys. Rev. Lett.* **77** (1996) 3865.
[110] J.P. Perdew, K. Burke, M. Ernyerhoh, *Phys. Rev. Lett.* **78** (1997) 1396.
[111] J.P. Perdew, J.A. Chevary, S.H. Vosko, K.A. Jackson, M.R. Pederson, D.J. Singh, C. Fiolhais, *Phys. Rev. B* **46** (1992) 6671.
[112] J.P. Perdew, J.A. Chevary, S.H. Vosko, K.A. Jackson, M.R. Pederson, D.J. Singh, C. Fiolhais, *Phys. Rev. B* **48** (1993) 4978.
[113] J.M. Perez-Jorda, E. San-Fabian, A.J. Perez-Jimenez, *J. Chem. Phys.* **110** (1999) 1916.
[114] W. Person, G. Zerbi, *Vibrational Intensities in Infrared and Raman Spectroscopy*, Elsevier, Amsterdam, 1982.
[115] K.A. Peterson, D.W. Woon, T.H. Dunning Jr., *J. Chem. Phys.* **100** (1994) 7410.
[116] P.L. Polavarapu, *J. Phys. Chem.* **94** (1990) 8106.
[117] J. Pu, J. Gao, D.G. Truhlar, *J. Phys. Chem. A* **108** (2004) 5454.
[118] E. Runge, E.K.U. Gross, *Phys. Rev. Lett.* **52** (1984) 997.
[119] K. Ruud, T. Helgaker, P. Bour, *J. Phys. Chem. A* **106** (2002) 7448.
[120] H. Rydberg, M. Dion, N. Jacobson, E. Schroeder, P. Hyldgaard, S.I. Simak, D.C. Langreth, B.I. Lundqvist, *Phys. Rev. Lett.* **91** (2003) 126402.
[121] P. Salek, O. Vahtras, T. Helgaker, H. Ågren, *J. Chem. Phys.* **117** (2002) 9630.
[122] D. Sanchez-Portal, P. Ordejon, E. Artacho, J.M. Soler, *Int. J. Quantum Chem.* **65** (1997) 453.
[123] O.F. Sankey, D.J. Niklewski, *Phys. Rev. B* **40** (1989) 3979.
[124] O.F. Sankey, D.J. Niklewski, D.A. Drabold, J.D. Dow, *Phys. Rev. B* **41** (1990) 12750.
[125] D.W. Schlosser, F.J. Devlin, K.J. Jalkanen, P.J. Stephens, *Chem. Phys. Lett.* **88** (1982) 286.
[126] J.C. Slater, *Phys. Rev.* **81** (1951) 385.
[127] J.M. Soler, E. Artacho, J.D. Gale, A. Garcia, J. Junquera, P. Ordejon, D. Sanchez-Portal, *J. Phys.: Condens. Matter* **14** (2002) 2745.
[128] F. Sottile, V. Olevano, L. Reining, *Phys. Rev. Lett.* **91** (2003) 056402.
[129] V.N. Staroverov, G.E. Scuseria, J. Tao, J.P. Perdew, *J. Chem. Phys.* **1190** (2003) 12129.
[130] P.J. Stephens, *J. Phys. Chem.* **89** (1985) 748.
[131] P.J. Stephens, *J. Phys. Chem.* **91** (1987) 1712.
[132] P.J. Stephens, C. Chabalowski, F.J. Devlin, K.J. Jalkanen, *Chem. Phys. Lett.* **225** (1994) 247.

[133] P.J. Stephens, K.J. Jalkanen, R.D. Amos, P. Lazzeretti, R. Zanasi, *J. Phys. Chem.* **94** (1990) 1811.
[134] P.J. Stephens, M.A. Lowe, *Annu. Rev. Phys. Chem.* **36** (1985) 213.
[135] V. Subramanian, D. Sivanesan, J. Padmanabhan, N. Lakshiminarayanan, T. Ramasami, *Proc. Indian Acad. Sci. (Chem. Sci.)* **111** (1999) 369.
[136] W.K. Surewicz, H.M. Mantsch, Infrared absorption methods for examining protein structure, in: *Spectroscopic Methods for Proteins in Solution*, VCH Publishers Inc., 69451 Weinheim, Germany, 1996, pp. 135–162.
[137] E. Tajkhorshid, K.J. Jalkanen, S. Suhai, *J. Phys. Chem. B* **102** (1998) 5899.
[138] L.G. Tensyeyer, E.W. Kauffman III, Protein structure as revealed by nonresonance Raman spectroscopy, in: *Spectroscopic Methods for Proteins in Solution*, VCH Publishers Inc., 69451 Weinheim, Germany, 1996, pp. 69–95.
[139] N. Troullier, J.L. Martins, *Phys. Rev. B* **43** (1991) 1993.
[140] S. Tsuzuki, H.P. Lüthi, *J. Chem. Phys.* **114** (2001) 3949.
[141] T. van Mourik, R.J. Gdanitz, *J. Chem. Phys.* **116** (2002) 9620.
[142] T. van Mourik, A.K. Wilson, T.H. Dunning Jr., *Mol. Phys.* **96** (1999) 529.
[143] P. van Remoortere, J.E. Mertz, L.E. Scriven, H.T. Davis, *J. Chem. Phys.* **110** (1999) 2621.
[144] I. Vasiliev, R.M. Martin, *Phys. Rev. A* **69** (2004) 052508.
[145] G. Vignale, M. Rasolt, D.J.W. Geldart, *Adv. Quantum Chem.* **21** (1990) 235.
[146] S.H. Vosko, L. Wilk, M. Nusair, *Cand. J. Phys.* **58** (1980) 1200.
[147] T.A. Wesolowski, Y. Ellinger, J. Weber, *J. Chem. Phys.* **108** (1998) 6078.
[148] A.K. Wilson, T. van Mourik, T.H. Dunning Jr., *J. Mol. Struct. (Theochem)* **288** (1996) 339.
[149] H.A. Witek, S. Irle, K. Morokuma, *J. Chem. Phys.* **121** (2004) 5163.
[150] H.A. Witek, K. Morokuma, *J. Comp. Chem.* **25** (2004) 1858.
[151] D.E. Woon, T.H. Dunning Jr., *J. Chem. Phys.* **100** (1994) 2975.
[152] Q. Wu, P.W. Ayers, W. Yang, *J. Chem. Phys.* **119** (2003) 2978.
[153] Q. Wu, W. Yang, *J. Chem. Phys.* **116** (2002) 515.
[154] X. Wu, M.C. Vargas, S. Nayak, V. Lotrich, G. Scoles, *J. Chem. Phys.* **115** (2001) 8748.
[155] X. Xu, W.A. Goddard III, *J. Phys. Chem. A* **108** (2004) 2305.
[156] X. Xu, W.A. Goddard III, *Proc. Natl. Acad. Sci.* **101** (2004) 2673.
[157] T. Yanai, D.P. Tew, N.C. Handy, *Chem. Phys. Lett.* **393** (2004) 51.
[158] T. Yanai, D.P. Tew, N.C. Handy, A new hydrid exchange-functional using the Coulomb-Attenuating Method (CAM-B3LYP). Response theory and molecular properties, Sønderborg, Denmark, May 2004.
[159] G.-S. Yu, T.B. Freedman, L.A. Nafie, T. Deng, P.L. Polavarapu, *J. Phys. Chem.* **99** (1995) 835.
[160] Y. Zhao, D.G. Truhlar, *J. Phys. Chem. A* **108** (2004) 6908.
[161] B.A. Zilles, W.B. Person, *J. Chem. Phys.* **79** (1983) 65.